Hurricane Track Prediction with a New Barotropic Model

HARRY C. WEBER

Meteorological Institute, University of Munich, Munich, Germany

(Manuscript received 2 October 2000, in final form 6 February 2001)

ABSTRACT

A new barotropic prediction system for the tracks of tropical cyclones is presented. The system (referred to as WBAR) consists of an initialization procedure, a vortex enhancement scheme, and a shallow water model, formulated in a geographical coordinate system. During model initialization, the operational wind field analyses and forecasts of a global model are postprocessed to remove unwanted features such as mislocated weak vortices. Then a synthetic vortex, constructed from the information given by operational tropical cyclone advisories, is implanted at the observed position. In the vicinity of the storm, the wind fields are modified such that the total flow at the storm center corresponds with the observed translation velocity. Geopotential height is adjusted to the wind field by solving a nonlinear divergence equation without the tendency term. The numerical model integrates the shallow water equations in a storm-relative circular domain over a period of 72 h, using the postanalyses of global model analyses and forecasts as time-dependent boundary conditions.

The present research version of WBAR has been developed on the basis of 167 cases (13 storms) during the 1996 Atlantic hurricane season, using predefined operational deep layer mean global model analyses and forecasts and tropical cyclone advisories of the U.S. National Centers for Environmental Prediction. The predicted 12-, 24-, 36-, 48-, 60-, and 72-h mean position errors in 1996, verified against best-track positions, are 78, 129, 184, 235, 295, and 360 km, respectively, with corresponding standard deviations of 40, 76, 111, 133, 168, and 182 km. At all prediction times except 12 h, WBAR has a consistent 30%–40% positive skill (defined as negative relative error) relative to CLIPER, a statistical regression model consisting of climatology and persistance predictors. With that, the performance of WBAR is comparable to that of the best track prediction model available in 1996, the Geophysical Fluid Dynamics Laboratory (GFDL) model.

In the 1996 Atlantic hurricane season, WBAR shows the following sensitivities: position errors are smaller than the mean position error of all 167 forecasts in the case of stronger storms, storms with smaller influence radii, storms at base date/time latitudes greater than about 15°, storms with higher translation speeds and, storms that move west- or northwestward. The seasonal performance is similar to that of VICBAR (Vic Ooyama's Barotropic Model), showing a decrease in skill later in the season. The new system has only a minor lack of skill relative to the GFDL model that results almost exclusively from three weak storms in 1996 (Gustav, Josephine, and Marco) and is possibly a consequence of inappropriate deep layer mean fields.

1. Introduction

Barotropic models have been used for predicting tropical cyclone tracks for more than three decades. Even during the last 10 years, when three-dimensional models have become very successful, barotropic models have still provided valuable operational guidance in tropical cyclone track prediction, at least over forecast periods of up to 48 h (DeMaria et al. 1992). The relative success of simple barotropic models, at least in the short-term track guidance, points to the possibility that an accurate representation of physical processes in complex three-dimensional numerical models may not be an absolutely necessary prerequisite for satisfactory track prediction (whereas the prediction of intensity is a different matter). The experiments with the new barotropic model discussed in the present study (henceforth referred to as WBAR) indicate that valuable track guidance is possible even over periods longer than 2 days, in contrast to common belief. Hence, simple models such as WBAR may not only prove to be useful for a number of research purposes, for example, for sensitivity studies of tropical cyclone track prediction, they may also form an attractive and equivalent alternative to more complex and computationally expensive three-dimensional models in operational forecasting, for example, for the production of statistical ensembles of track predictions.

The first operational barotropic model used for tropical cyclone track prediction (Sanders Barotropic Hurricane Track Forecast Model, SANBAR) was developed by Sanders and Burpee (1968) and became operational at the National Hurricane Center (NHC) in Miami, Florida, in the late 1960s (Sanders et al. 1975). The model was based on the traditional view that to a first approximation, tropical storm motion follows a deep layer

Corresponding author address: Harry C. Weber, Meteorological Institute, University of Munich, Theresienstr. 37, 80333 Munich, Germany.
E-mail: harry@meteo.physik.uni-muenchen.de

TABLE 1. Major technical features of VICBAR and WBAR.

	VICBAR	WBAR
Input datasets	Predefined NCEP DLMs 850–200 hPa; 27.5°S–67.5°N, 140°W–10°E; NCEP TC advisory	Predefined NCEP DLMs 850–200 hPa; 27.5°S–67.5°N, 140°W–10°E, NCEP TC advisory
Additional datasets	Rawinsondes, satellite cloud track winds, aircraft observations	None
Synthetic vortex	DeMaria et al. [1992, Eq. (3.8)] and constant vector representing the initial storm motion, blended with the analysis within a circle of 600 km	DeMaria et al. [1992, Eq. (3.8)] and adjustment of the flow at the vortex center to the observed motion, added to the analysis within a circle of radius R (see section 3c)
Governing equations	Shallow-water, Mercator projection, spline representation, triply nested, inner nests movable	Shallow-water, lat–long grid, finite differences, no nesting
Horizontal resolution	0.6°, 1.2°, 2.4°, and 4.8° in lat–long	0.5° in lat–long
Mean fluid depth	750 m	750 m
Barotropic integration domain	Circular $r \leq 1500$ km: purely barotropic $r > 1500$ km: adjustment to baroclinic DLMs via nudging terms in the governing equations	Circular, storm-dependent (section 4b) $r \leq R_A$: purely barotropic $R_A < r \leq R_B$: adjustment to baroclinic DLMs via weights $r > R_B$: purely baroclinic DLMs
Boundaries	Time dependent, if possible	Time dependent
Geopotential height	Divergence equation, divergence and divergence tendency set to zero	Divergence equation, divergence tendency set to zero

mean (DLM; defined as a mass-weighted vertical average of meteorological variables) ''steering flow,'' in which the storm is embedded. Storm tracks were predicted by integration of the barotropic vorticity equation, using initial streamfunction and relative vorticity distributions derived from DLM wind fields. As in current practice (cf. section 3), storms were represented by synthetic symmetric vortices, including an azimuthal wavenumber one streamfunction pattern that matched the existing streamfunction to that representing the current translation velocity of the storms. Within a predefined radius from the observed storm center, the original vorticity and streamfunction distributions were replaced by those of the synthetic vortex. In spite of the relative paucity of meteorological measurements over the Atlantic Ocean compared with today and the relatively coarse numerical grid size (154 km), SANBAR produced astonishingly good track predictions that were as skillful (for the definition of skill see the appendix) as those of models using climatology and persistence predictors, for example, the Hurricane Analog Scheme (HURRAN; Hope and Neumann 1970) and the Climatology and Persistence Scheme (CLIPER; Neumann 1972). In 1973, for example, the 72-h mean position errors of SANBAR were 750 and 900 km in homogeneous comparisons with those of HURRAN and CLIPER, respectively (Sanders et al. 1975, p. 277).

Refinements of SANBAR in the 1970s and 1980s included the use of aircraft winds and satellite-derived cloud-drift vectors (Sanders et al. 1980), the use of omega dropwindsondes (ODW; Goldenberg et al. 1985) or the Visible/Infrared Spin-Scan Radiometer (VISSR) Atmospheric Sounder (Lewis et al. 1985). These modifications led to a slight improvement of track prediction with SANBAR and to positive skill relative to CLIPER. A substantial improvement of the track prediction with SANBAR was achieved by Goldenberg et al. (1987), using a finer grid size and an initialization strategy similar to that presented in this paper (cf. section 3). In contrast to the former version of SANBAR, Goldenberg et al. blended the large-scale vorticity field smoothly with that of a synthetic symmetric vortex including its asymmetries. Position errors of a homogeneous sample of cases between 1979 and 1982 showed an improvement of more than 10% compared with the operational SANBAR (e.g., from 713 to 651 km at 72 h).

One of the most successful barotropic models for tropical cyclone track prediction to date is the nested spectral model of Vic Ooyama (VICBAR; DeMaria et al. 1992). On an experimental basis, it replaced SANBAR as the operational track prediction model for the Atlantic basin in 1989. The VICBAR prediction system uses cubic B-spline representations of all variables for the initialization procedure as well as for the time integration of the shallow-water equations on a Mercator projection. The model equations are solved on a sequence of vortex-relative nested meshes with successively increased resolution. A list of the main features of VICBAR is given in Table 1. As in the new barotropic track prediction system WBAR (cf. also Table 1), VICBAR uses 850–200-hPa DLM analyses and forecasts of a global spectral model [the National Centers for Environmental Prediction's (NCEP) Aviation Model] as initial conditions and time-dependent boundary conditions (since 1990) such that outside a predefined circle about a storm center, the barotropic forecasts are successively adjusted to the baroclinic forecasts. Besides global model analyses and forecasts, VICBAR uses rawinsonde data, satellite cloud-track winds, and special aircraft observations for its initialization. Based on op-

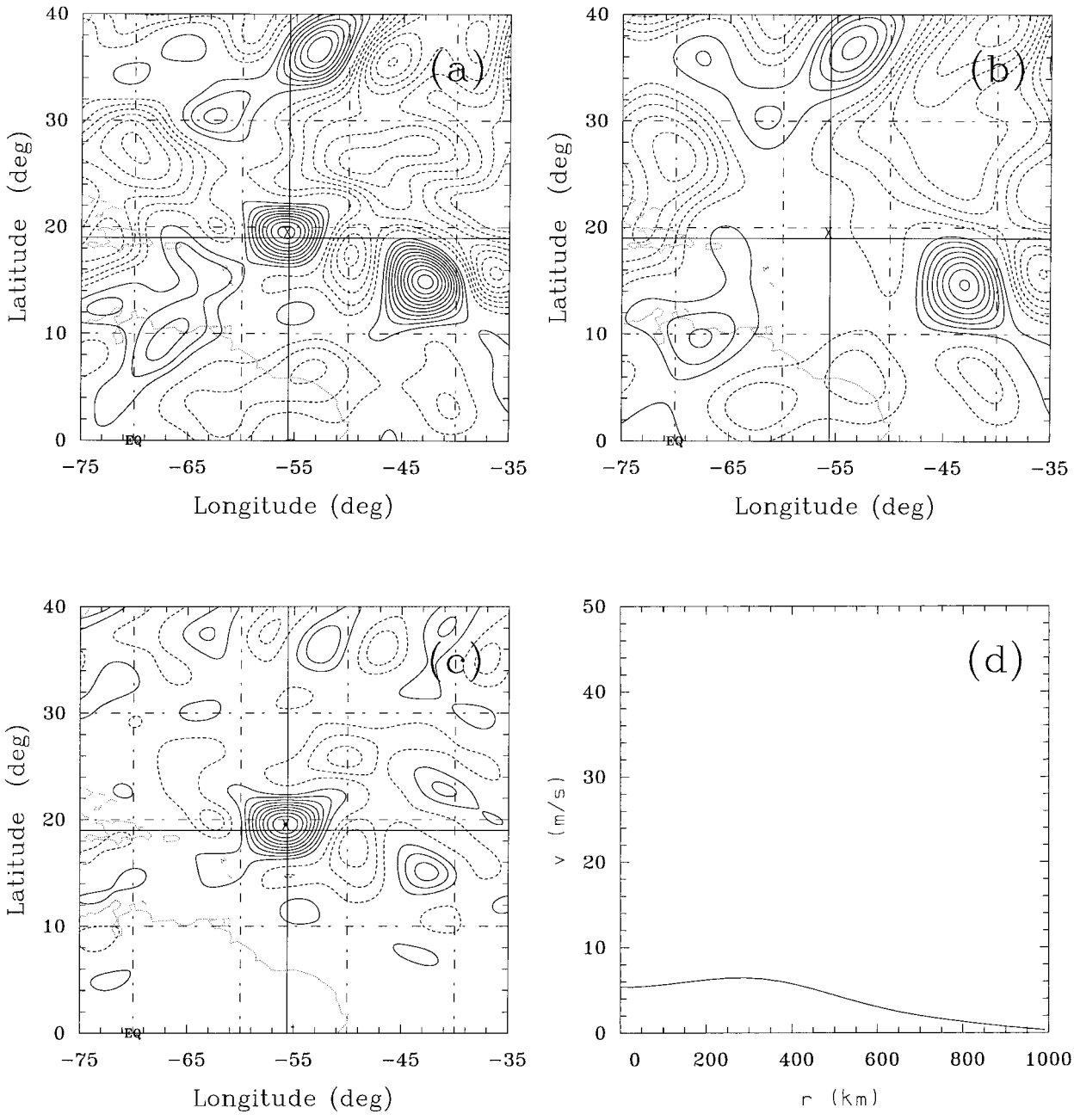

FIG. 1. Postanalysis of Hurricane Edouard at 0000 UTC 27 Aug 1996. (a) Original relative vorticity ζ of the NCEP global model, (b) large-scale environment of relative vorticity ζ^{EL}, (c) residual relative vorticity ζ^{R}, (d) symmetric tangential wind v^{VS} as a function of radius, (e) wavenumber one relative vorticity ζ^{VA}, and (f) total environment of relative vorticity ζ^{E}. Continents are outlined in dotted contours. The intersection of axes represents the observed center and X marks the center of the resolved vortex in the global model analysis. Contour intervals in the vorticity plots are 5×10^{-6} s^{-1} in (a), (b), (c), and (f) and 1×10^{-6} s^{-1} in (e). Negative values are dashed. Note that the slightly square structure of Edouard, e.g., in (a) or in Fig. 2c, is caused by using the 2.5° grid for plotting; in the initial fields of the numerical model, storms are axisymmetric due to direct interpolation of the radial distribution of the synthetic vortex to the model grid.

erational tropical cyclone (TC) advisories, an artificial symmetric vortex, and a constant wind vector (the latter representing the observed translation velocity) are constructed and blended with the objective analysis of the global model. Verification of the results of VICBAR showed that, with mean position errors of 358 (573) km at 48 (72) h, it compared well with all other operational models between 1989 and 1993 (Aberson and DeMaria 1994). Especially in cases of strong storms, VICBAR provided excellent track guidance. However, Aberson and DeMaria showed also that position errors increased as the hurricane season progressed, possibly in response

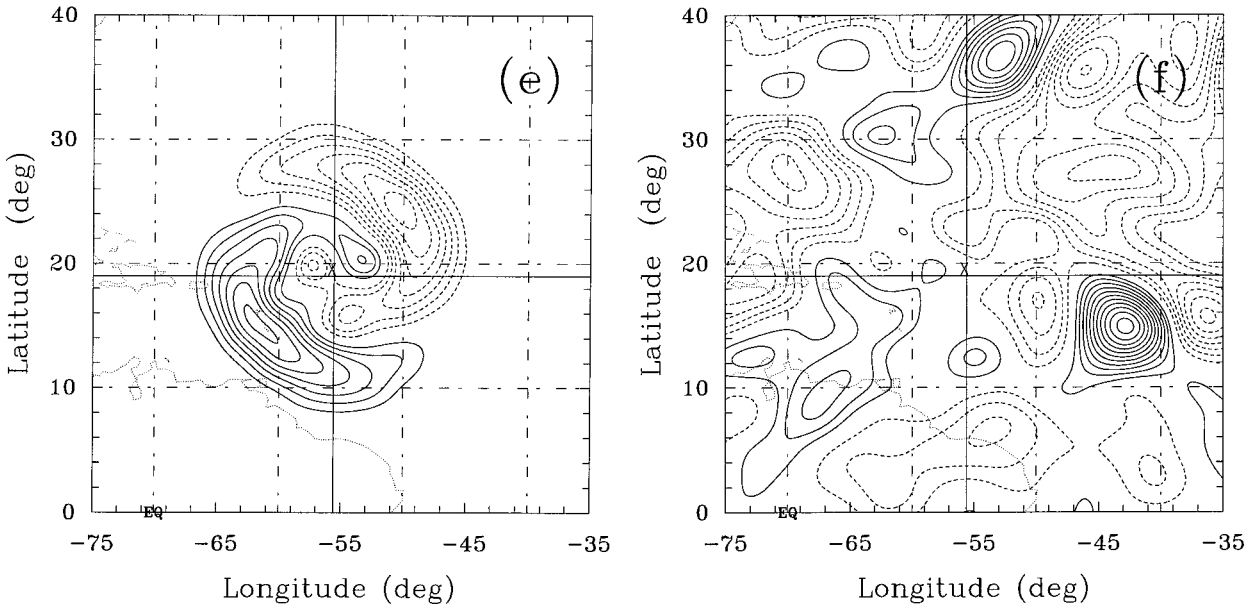

FIG. 1. (*Continued*)

to baroclinic systems extending farther south in autumn than in summer. Furthermore, the VICBAR position errors were found to depend on latitude and longitude, with smaller errors south of 18°N and north of 33°N and east of the Caribbean Sea and Bermuda. The large errors in the latitudinal band between 18° and 33°N were attributed mainly to cases of recurving storms. Finally, VICBAR position errors seemed to be consistently large in cases of interaction between closely located storms and in cases of storms in high vertical wind shear.

In 1996, a new barotropic numerical model, the Limited-Area Sine Transform Barotropic Track Model, (LBAR), was implemented operationally (Horsfall et al. 1997). The LBAR model is based on VICBAR and was developed as a full operational version of VICBAR, but with a different and simpler numerical solution method (harmonic sine series expansion instead of cubic B-splines). In spite of this simplification, the quality of track guidance provided by LBAR is comparable to that of VICBAR or even better. However, in the 1996 hurricane season, the period of interest here, the performance of LBAR is slightly worse than that of VICBAR [e.g., the 48- and 72-h mean position errors of LBAR (VICBAR) are 304 (301) and 559 (544) km]. Therefore, LBAR is not used for a comparison with WBAR in the present paper.

During the 1990s, the development of sophisticated three-dimensional regional models such as the Geophysical Fluid Dynamics Laboratory (GFDL) model (Kurihara et al. 1993, 1995, 1998; Bender et al. 1993, and references contained therein), the Japan Meteorological Agency (JMA) model (Ueno 1989), or the Limited Area Prediction System (LAPS; Davidson and Puri 1992; Davidson et al. 1993) and TC-LAPS (Davidson and Weber 2000) of the Australian Bureau of Meteorology (BoM) led to a general improvement of tropical cyclone track guidance. Furthermore, in recent years global models such as the NCEP model (Surgi et al. 1998), the U.K. Met. Office (UKMO) model (Heming and Radford 1998), and the European Centre for Medium-Range Weather Forecasts (ECMWF) model provided much better forecast guidance, possibly also as a result of recent developments in computer technology that allow weather predictions at higher resolution than before. As a consequence, it is widely accepted that barotropic models are no longer competitive, at least with respect to medium-range track prediction over periods longer than 48 h. As will be shown in the present paper, this opinion may need to be reconsidered, because barotropic models *are* capable of producing valuable track guidance even for prediction periods longer than 48 h.

Mostly as a result of the still inadequate distribution of meteorological measurements in the vicinity of tropical cyclones, the models discussed above (except the ECMWF model) apply more or less complex methods of vortex specification during their initialization. For example, in VICBAR (DeMaria et al. 1992) and the UKMO model (Heming and Radford 1998) a symmetric model storm, together with a constant wind field representing the current translation velocity of the storm, is specified and merged with the other datasets used during initialization inside a circle about the observed storm position. More sophisticated initialization procedures are used in track and intensity prediction systems like the GFDL model (cf. Kurihara et al. 1993) or TC-LAPS (Davidson and Weber 2000). The ideas applied in these two models are similar, but they have

TABLE 2. Summary of all 1996 Atlantic storms. The second column represents the periods where datasets were available. Columns three–six show the range of v_m in m s^{-1}, r_i in km, ϕ_c in ° latitude (for definitions see section 2), and the directions of motion during the periods of interest. The last column gives the approximate location where tropical storm strength was reached [source: Pasch and Avila (1999) and operational NCEP TC advisories].

Storm	Time (UTC) date	v_m	r_i	ϕ_c	c_d	Origin
Arthur	1200 18 Jun–1200 20 Jun	15–18	220–280	30–37	N–NE	E of Georgia
Bertha	1200 5 Jul–1200 13 Jul	18–51	280–370	10–39	WNW–NW–NE	Mid-Atlantic
Cesar	0000 26 Jul–1200 27 Jul	21–33	280–560	11–13	W	N of Venezuela
Dolly	0000 20 Aug–0000 23 Aug	15–33	230–330	18–21	WNW	W of Jamaica
Edouard	0000 22 Aug–1200 2 Sep	15–64	370–560	13–40	W–N–NE	W of Cape Verde
Fran	1200 24 Aug–0000 6 Sep	15–51	280–460	14–34	W–NW	Mid-Atlantic
Gustav	1200 28 Aug–1200 1 Sep	15–21	220–280	11–20	W–NW	WSW of Cape Verde
Hortense	1200 5 Sep–0000 15 Sep	13–62	230–500	14–45	WNW–N–NE	E of Guadeloupe
Isidore	0000 25 Sep–0000 1 Oct	15–51	230–330	10–30	W–N–NE	SW of Cape Verde
Josephine	1200 5 Oct–0000 8 Oct	15–31	220–560	23–29	NE	W Gulf of Mexico
Kyle	0000 12 Oct	23	220	17	SW	E of Belize
Lili	1200 15 Oct–1200 26 Oct	15–51	370–670	16–41	NW–NE	NW of Honduras
Marco	1200 19 Nov–1200 26 Nov	15–33	230–560	14–20	SW–E–NE–W–NW	E of Nicaragua

been developed independently of each other and differ in some significant aspects. As the vortex specification method of TC-LAPS forms the basis of the method used in the new barotropic track prediction system discussed in this paper, it will be summarized briefly: the synthetic symmetric vortex is computed using a modification of the vortex enhancement scheme discussed in Davidson et al. (1993). Artificial vortex asymmetries are constructed on the basis of the extended analytical theory of vortex motion of Smith and Weber (1993). They are adjusted such that the sum of all induced flows across the vortex center, calculated using an arbitrary flow partitioning into contributions of smaller and larger horizontal scale, matches the observed translation velocity of a given storm.[1] The artificial observations are blended with the original observations and an optimum interpolation objective analysis is carried out to generate the initial condition for the prediction model. Finally, 24 h of diabatic, dynamical nudging (Davidson and Puri 1992; Davidson and Weber 2000) through 6-hourly objective analyses (including the synthetic vortex) is carried out. During the nudging period, the original vorticity and surface pressure distributions are largely preserved, while satellite cloud imagery is used to adjust the vertical motion field.

At present it is commonly accepted that track predictions of high quality may be achieved only by vortex specification. Based on the ideas of some of the numerical models described above, especially the initialization strategy of TC-LAPS, the analysis concept developed by Weber and Smith (1995) and the (unsuccessful) attempt to improve track prediction with VICBAR [together with S. Aberson of the National Oceanic and Atmospheric Administration's Hurricane Research Division (HRD)] by modification of its initialization method, a research version of the new barotropic track prediction system WBAR has been developed and is presented in the following sections. The results of extensive tests, optimization strategies, and sensitivity experiments, carried out for all 13 Atlantic storms of 1996, demonstrate the potential of WBAR to accurately predict tropical cyclone tracks over periods longer than 48 h. In view of a possible operational application in the future, further tests and long-term statistical evaluations are planned, to assess the consistency of the WBAR performance for different seasons and geographical regions. The forecast failures of WBAR, initialized with NCEP operational predefined 850–200-hPa DLM global analyses and forecasts, *without* additional input such as ODW or aircraft observations, point toward possibilities of further substantial improvements of barotropic tropical cyclone track forecasting.

2. Datasets

All experiments and tests with WBAR have been carried out using tropical cyclone events at 167 base dates/times (either 0000 or 1200 UTC) of all 13 storms occurring during the 1996 Atlantic hurricane season (for a brief summary of these storms see Table 2). The basic datasets used for the initial conditions and the time-dependent boundary conditions of the prediction model consist of *predefined* 850–200-hPa DLM wind and height operational objective analyses and forecasts of the 1996 NCEP global model. Geopotential height is provided in the form of height deviations from a mean distribution. The datasets cover a region between 140°W and 10°E in longitude λ and 27.5°S and 67.5°N in latitude φ, that is, the whole North Atlantic Ocean and its surrounding area. The horizontal grid size is 2.5° in latitude and longitude. The datasets were provided by S. Aberson of the HRD and are exactly the same as those used by the semioperational VICBAR (Table 1; cf. also DeMaria et al. 1992, p. 1634) since the year 1991.

[1] Hence, these asymmetries do not necessarily correspond with β gyres (cf., e.g., Holland 1983; Chan and Williams 1987; Fiorino and Elsberry 1989) as in a former version of the GFDL model (Kurihara et al. 1993).

TABLE 3. Abbreviations and definitions used in section 3.

Abbreviation	Explanation
$\mathbf{F}$	Original global input zonal and meridional wind
$\mathbf{F}^E$	Environmental contribution to $\mathbf{F}$, $\mathbf{F}^E = \mathbf{F}^{EL} + \mathbf{F}^{ES}$
$\mathbf{F}^V$	Vortex contribution to $\mathbf{F}$, $\mathbf{F}^V = \mathbf{F}^{VS} + \mathbf{F}^{VA}$
$\mathbf{F}^{EL}$	Contribution to $\mathbf{F}^E$ of larger horizontal scale than the vortex
$\mathbf{F}^{ES}$	Contribution to $\mathbf{F}^E$ of same or smaller horizontal scale than the vortex, $\mathbf{F}^{ES} = \mathbf{F}^R - \mathbf{F}^{VS} - \mathbf{F}^{VA}$
$\mathbf{F}^{VS}$	Mispositioned symmetric contribution to $\mathbf{F}^V$
$\mathbf{F}^{VA}$	Asymmetric contribution to $\mathbf{F}^V$ relative to center of $\mathbf{F}^{VS}$
$\mathbf{F}^R$	Residual field, $\mathbf{F}^R = \mathbf{F} - \mathbf{F}^{EL}$
$\mathbf{F}^{BS}$	Synthetic symmetric vortex, computed using TC advisory
$\mathbf{F}^{BO}$	Final synthetic symmetric vortex, merged from $\mathbf{F}^{BS}$ and $\mathbf{F}^{VS}$
$\mathbf{F}^M$	Adjustment field (synthetic vortex asymmetries)
$\mathbf{F}^O$	Global output field, $\mathbf{F}^O = \mathbf{F}^E + \mathbf{F}^{BO} + \mathbf{F}^M$, replaces $\mathbf{F}$

Besides the DLM analyses and forecasts of the NCEP global model, operational NCEP TC advisories (provided also by S. Aberson) were used for the construction of synthetic storms and the incorporation of translation velocities in the initial fields of the numerical model (cf. section 3). Again, these datasets are exactly the same as those used by VICBAR for track prediction (cf. Table 1). The TC advisories provide information about base dates/times t_0, storm positions (latitudes φ_c and longitudes λ_c) at t_0, $t_0 - 12$ and $t_0 - 24$ h, radii of maximum tangential wind speed r_m, radii of the outermost closed isobar r_i (henceforth referred to as influence radii), maximum wind speeds v_m at t_0 and at $t_0 - 12$ h, current translation directions[2] c_d, and translation speeds c. A summary of the range of these parameters during the time periods where storms existed in the Atlantic and datasets were available is given in Table 2.

It should be noted that no additional datasets such as rawinsonde observations, satellite cloud-track winds or special aircraft observations as, for example, ODWs were incorporated during the initialization of WBAR. These datasets are used by VICBAR (cf. DeMaria et al. 1992; Aberson and DeMaria 1994), but were not available for the experiments described in this paper.

The storm positions predicted with WBAR were verified against best-track positions available online (http://www.weather.unisys.com). Position errors were computed using spherical geometry. Furthermore, predicted 12-, 24-, 36-, 48-, and 72-h storm positions of all operational models and the official NHC forecasts of the 1996 Atlantic hurricane season[3] were made available by S. Aberson.

3. Model initialization

This section gives an overview of the present optimum initialization procedure of the research version of WBAR, developed in a large number of experiments using different initial configurations and concepts of initialization for all 167 cases of the 1996 Atlantic hurricane season. The more important methods of initialization that did not produce adequate forecast results in comparison with the current one are addressed briefly in section 5. The separate steps of the initialization procedure are exemplified by Figs. 1 and 2, showing DLM relative vorticity and tangential wind distributions for the case of Hurricane Edouard on 27 August 1996 at 0000 UTC. All definitions used in this section are listed in Table 3.

The initialization procedure consists of a postanalysis of the predefined 850–200-hPa DLM wind components of the operational objective analyses and forecasts of the NCEP global model and the construction of a synthetic vortex using the information provided by the operational TC advisories. The postanalysis is carried out separately for the NCEP global model analyses at $t = t_0 - 12$ and t_0 h and forecasts at $t = t_0 + 12$, $t_0 + 24$, . . ., $t_0 + 72$ h. The analysis procedure is based on the methodology discussed in Weber and Smith (1995) and is similar to the operational vortex enhancement scheme used in TC-LAPS (Davidson and Weber 2000). Its aim is to carefully remove unwanted features from the NCEP global model analyses and forecasts such as mislocated, comparably large, and (not necessarily) weak vortices that may represent a resolved storm circulation in the NCEP global model datasets. Keeping these resolved

[2] The original translation direction in the TC advisories is defined in a clockwise sense relative to an axis pointing northward. Throughout the present paper, this definition is changed and c_d is defined in a counterclockwise sense relative to an axis pointing eastward.

[3] Note that the predicted storm positions of the 1996 operational models at 60 h were not available.

TABLE 4. Values of radii r_1 and r_2 of the contributions $\mathbf{F}^{VS}$ and $\mathbf{F}^{VA}$ as multiples of the operational influence radius r_i (or $r_i^* = 1.5\ r_i$) and dependence on the maximum wind speed provided by the TC advisory.

		Global model analyses		Global model forecasts	
		r_1 ($\times\ r_i^*$ in km)	r_2 ($\times\ r_i^*$ in km)	r_1 ($\times\ r_i^*$ in km)	r_2 ($\times\ r_i^*$ in km)
u^{VS}, v^{VS}		1	3	1	3
u^{VA}, v^{VA}	$v_m < 38$ m s^{-1}	0	1	0	1
	$v_m \geq 38$ m s^{-1}	1	2	0	1

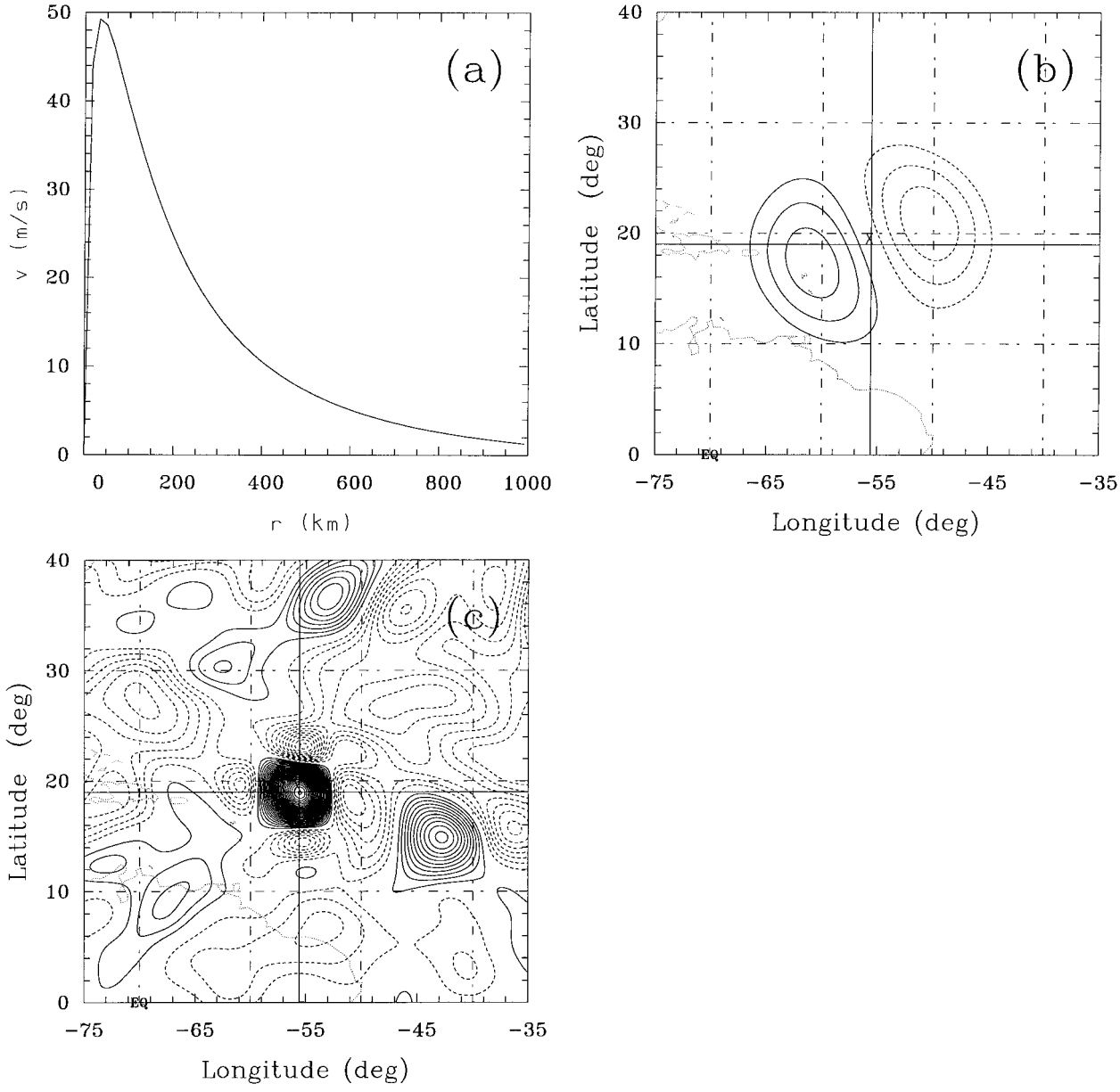

FIG. 2. As in Fig. 1 but for (a) symmetric synthetic tangential wind v^{BO}, (b) adjustment field of relative vorticity ζ^{M}, and (c) total output field of relative vorticity ζ^{O}. Contour intervals in the vorticity plots are 1×10^{-6} s^{-1} in (b) and 5×10^{-6} s^{-1} in (c).

storms in the initial fields and in the time-dependent boundary conditions of the numerical model may cause serious problems during the track prediction, in the worst case vortex–vortex interaction. On the other hand, the goal is also to keep modifications of the NCEP global model analyses and forecasts by the postanalysis to a minimum, in order to retain as much information in the global model datasets as possible.

The postanalysis of the analyses and forecasts of the NCEP global model is carried out for the zonal and meridional wind only and is based on an arbitrary partitioning of these fields, following Weber and Smith (1995; cf. also Kurihara et al. 1993). Figure 1a shows an example of a DLM relative vorticity distribution as provided by the NCEP global model. Note the displacement of the storm in the NCEP global model analysis (marked by X) relative to the observed position (indicated by the cross hairs). The zonal and meridional wind (U, V) or the radial and tangential wind (u, v), henceforth defined by the vector field $\mathbf{F}$, is partitioned into an environmental component $\mathbf{F}^{E}$ and a vortex component $\mathbf{F}^{V}$ such that $\mathbf{F} = \mathbf{F}^{E} + \mathbf{F}^{V}$. The two components are further subpartitioned into $\mathbf{F}^{E} = \mathbf{F}^{EL} + \mathbf{F}^{ES}$ and $\mathbf{F}^{V} = \mathbf{F}^{VS} + \mathbf{F}^{VA}$, where $\mathbf{F}^{EL}$ and $\mathbf{F}^{ES}$ represent features of

larger and the same or smaller horizontal scale than that of the storm (defined by r_i). Here, $\mathbf{F}^{VS}$ and $\mathbf{F}^{VA}$ represent the resolved symmetric storm in the NCEP global model data and its asymmetries,[4] respectively. The basic assumption in the case of $\mathbf{F}^{VA}$ is that it is generated, at least in part, by the resolved vortex in the NCEP global model analyses/forecasts due to its motion during the data assimilation process or the global model forecast.

a. Extraction of the large-scale environment $\mathbf{F}^{EL}$

Prior to the extraction of the large-scale environment $\mathbf{F}^{EL}$, the resolved vortex is temporarily removed from the NCEP global model analyses by application of a simple four-point smoother to $\mathbf{F}$ in a $20° \times 20°$ latitude–longitude domain centered approximately at the observed storm center. The reason for the use of the four-point filter is that parts of the resolved storm would remain in the final $\mathbf{F}^{EL}$ in response to the filter characteristics of the method described below, if applied directly to $\mathbf{F}$. The current value of 20° has been chosen such that even the largest storms of 1996 (e.g., Lili with $r_i = 670$ km), that is their representations in the NCEP global model analyses and forecasts,[5] lie completely inside the smoothing domain. In this way, the presmoothing ensures that the final $\mathbf{F}^{EL}$ varies smoothly over the size of the resolved vortex in the NCEP global model analyses and forecasts.

After the smoothing, $\mathbf{F}^{EL}$ is extracted with a modified Barnes scheme (Barnes 1964; Weber and Smith 1995, p. 637f) in combination with a low-pass filter in the form of a one-dimensional fast Fourier transform (Press et al. 1986, p. 495ff). The filter successively removes waves with wavelengths greater than a given truncation wavelength, $\Lambda_t = 4r_i$. (Note that the iterative Barnes method does not sharply eliminate all waves of wavelengths shorter than Λ_t. It produces a spectrum of waves of shorter and longer wavelengths that smoothly decrease in magnitude with decreasing wavelength.) The numerical value of Λ_t has been found in a number of sensitivity tests and approximately represents an optimum value. The particular filter characteristics of the low-pass filter and the convergence of meridians in the geographical grid require the formulation of a new grid in an equidistant Cartesian coordinate system within the original geographical grid. The new grid is centered approximately on the observed storm position and has a size of 7000 km × 7000 km, with a horizontal grid size of 250 km. In cases where the storm is located near the boundaries of the global model analysis and forecasts, however, the Cartesian grid system can be repositioned and/or decreased in size such that it fits completely in the 2.5° domain. The wind fields are interpolated to the new grid by birational interpolation (Späth 1991; Weber and Smith 1995, p. 636), with distances measured using spherical geometry. The low-pass filter is applied alternately to all row and column vectors of U and V in the new grid. After reinterpolation to the 2.5° grid, $\mathbf{F}^{EL}$ forms a smooth and slowly varying background in contrast to $\mathbf{F}$ as documented by the relative vorticity distribution shown in Fig. 1b. It is stored for later use and subtracted from $\mathbf{F}$ to produce a residual field $\mathbf{F}^{R}$ (Fig. 1c; cf. also Kurihara et al. 1993), which is subjected to the azimuthal analysis described below.

b. Search for the center of the resolved vortex in $\mathbf{F}^{R}$

Prior to an azimuthal analysis, the center of the resolved vortex, (λ_m, φ_m), defined by the maximum (minimum) of the vertical component of relative vorticity in the Northern (Southern) Hemisphere, has to be located in $\mathbf{F}^{R}$. In the NCEP global model analyses, the observed position is used as first guess for the center search. In the NCEP forecasts, the center of the storm in the previous analysis or forecast is used as a first guess, but the new center must lie within a 90° angle centered either in the observed translation direction or in the direction of the difference vector between the centers found in the two fields analyzed earlier. The center can be located with satisfactory accuracy (presently 500 m) by combination of birational interpolation (Späth 1991) with a ''downhill method'' (Bach 1969). The downhill method (cf. also Weber and Smith 1993) locates the minimum of an analytic two-dimensional function (given here by the interpolation coefficients) by successive changes of λ and φ using a range of walk patterns. If no center can be detected, no azimuthal analysis is carried out and the original analyses or forecasts remain unchanged.

c. Azimuthal analysis of $\mathbf{F}^{R}$ and restoration of the total environment $\mathbf{F}^{E}$

First, (U^R, V^R) are transformed to radial and tangential wind fields (u^R, v^R) relative to (λ_m, φ_m). Within a circle of maximum radius R that fits completely in the Cartesian grid, u^R and v^R are subjected to an azimuthal Fourier analysis about (λ_m, φ_m) to produce axisymmetric and azimuthal wavenumber one radial and tangential winds $\mathbf{F}^{VS}$ and $\mathbf{F}^{VA}$ as a function of radius r (see footnote 4, and Davidson and Weber 2000, their appendix). Higher wavenumber contributions are not computed because of the limited horizontal resolution of the NCEP global model analyses and forecasts and because they do not have a direct effect on storm motion (cf., e.g., Fiorino and Elsberry 1989).

Before their elimination from $\mathbf{F}^{R}$, $\mathbf{F}^{VS}$, and $\mathbf{F}^{VA}$ are smoothed such that they tend to zero between two radii r_1 and r_2 with $r_1 < r_2 < R$, using a filter of the form

[4] Defined as azimuthal wavenumber one asymmetry of u and v. Note that wavenumber one (u, v) fields transform into wavenumber zero and two (U, V) fields, because $U(r, \theta, t) = u(r, \theta, t)\cos(\theta) - v(r, \theta, t)\sin(\theta)$ and $V(r, \theta, t) = u(r, \theta, t)\sin(\theta) + v(r, \theta, t)\cos(\theta)$. Here, r is radius, θ is azimuthal angle, and t is time.

[5] The resolved storms in the global analyses and forecasts are generally larger in size in comparison with the observed storm size given by r_i.

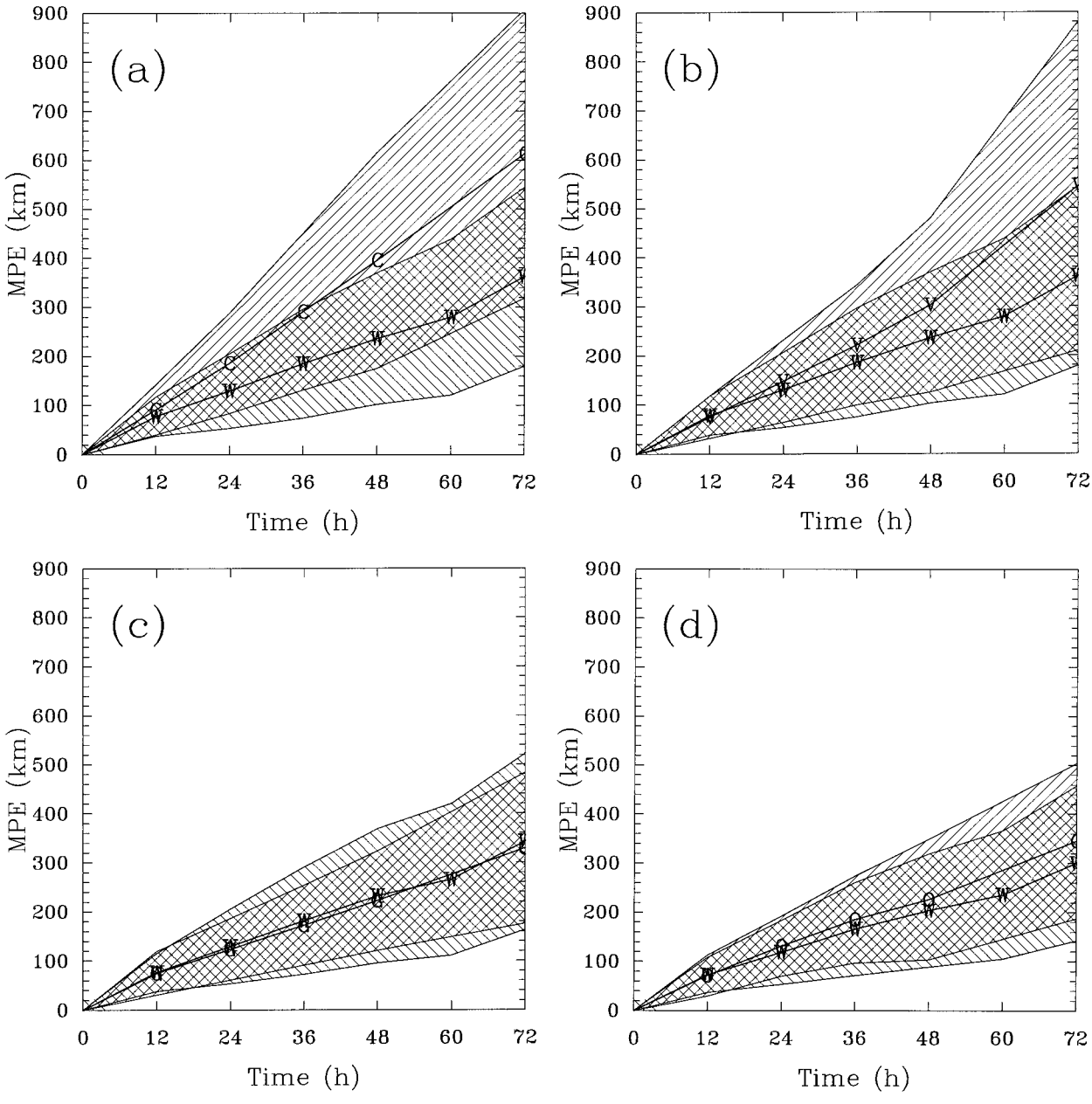

FIG. 3. MPEs in km at all prediction times of WBAR and (a) CLIPER (C), (b) VICBAR (V), (c) the GFDL model (G), and (d) the official forecasts of the NHC (O). The shaded areas represent the 66.6% σ values of the standard deviation in km of WBAR (\\\\) and the other models (////) at all prediction times. Note that the 60-h MPEs of CLIPER, VICBAR, the GFDL model, and the official NHC forecasts were not available.

$[1 - s^2 \exp(1 - s^2)]$, where $s = (r - r_1)/(r_2 - r_1)$ and $r_1 \le r \le r_2$. The choice of r_1 and r_2 has a major effect on the predicted tracks, because these radii control the structure of $\mathbf{F}^{VA}$ that remains in the initial wind fields of the numerical model and directly governs storm motion. In principal, there is no unique way to distinguish between a wavenumber one feature that is generated in response to vortex motion during a global model objective analysis cycle or forecast and a wavenumber one feature that results from the synoptic situation in which the storm is embedded. For example, if a given storm is located in the vicinity of a trough, the trough would form a wavenumber one perturbation to the vortex in the prediction model and would govern its subsequent motion; if too much of the trough is removed from the initial fields, track prediction may fail. Based on these reflections and on the assumption that stronger storms have a greater influence on their environment, while

TABLE 5a. Homogeneous comparison of WBAR with CLIPER at all prediction times. MPE: mean position errors in km of CLIPER (CLIP) and WBAR, using all available CLIPER forecasts (comp) and distinct subsets at 0000 UTC (0000 UTC) and 1200 UTC (1200 UTC); SD: 66.6% σ value of the standard deviation in km; *S*: skill in % (negative values denote positive skill); *N*: total number of cases; NWB: percentage of cases where WBAR performed better than CLIPER. Asterisks represent MPEs that were found to be significantly different from those of CLIPER at the 95% level of a paired Student's *t* test.

Prediction time (h)			12	24	36	48	60	72
MPE (km)	CLIP		91	185	289	393	—	607
	WBAR	comp	77*	129*	185*	236*	296*	361*
		0000 UTC	76*	128*	181*	241*	311*	364*
		1200 UTC	79*	131*	188*	230*	283*	359*
SD (km)	CLIP		51	102	159	218	—	292
	WBAR		40	76	110	133	168	182
S (%)			−14.5	−30.2	−36.1	−40.0	—	−40.5
N			166	154	143	131	119	108
NWB (%)			63	70	69	74	—	69

weaker storms are affected to a greater extent by the surrounding flow, optimum storm-dependent values of r_1 and r_2 as functions of r_i (or $r_i^* = 1.5r_i$) and v_m have been determined in sensitivity experiments using all 167 available base dates/times of the 1996 hurricane season. However, we are aware that further tests, using a large number of storms in different seasons and different regions, are required to test the general validity of the above parameters and all other parameters used during initialization (see below) and in the numerical model (see section 4). The current values of r_1 and r_2 are given in Table 4. Examples of v^{VS} and the asymmetric relative vorticity distribution are shown in Figs. 1d and 1e, respectively.

After retransformation of (u, v) to (U, V), the smoothed functions $\mathbf{F}^{VS}$ and $\mathbf{F}^{VA}$ are subtracted from $\mathbf{F}^{R}$ to produce $\mathbf{F}^{ES}$. In an effort to retain a maximum amount of the original information and based on the assumption that the symmetric circulation projected onto the azimuthal average is well resolved in the NCEP global model analysis at large radii, $\mathbf{F}^{VS}$ is stored for blending with the synthetic symmetric vortex constructed later, while $\mathbf{F}^{VA}$ is regarded exclusively as a numerical artifact of NCEP global model data assimilation or forecast and is not stored. Addition of $\mathbf{F}^{EL}$ and $\mathbf{F}^{ES}$ yields the total environment $\mathbf{F}^{E}$ shown by the relative vorticity distribution of Fig. 1f, which now includes also features of the same or smaller horizontal scale than the scale of the symmetric vortex $\mathbf{F}^{VA}$ in the vicinity of the storm.

d. Symmetric vortex specification

The synthetic symmetric vortex $\mathbf{F}^{BS}$ is computed only for the NCEP global model analyses. The construction of $\mathbf{F}^{BS}$ is carried out using the storm parameters provided by the operational TC advisory. With a few exceptions, the synthetic vortex is exactly the same as the one used in VICBAR [cf. Table 1; see also DeMaria et al. 1992, their Eq. (3.8), and the following paragraph] and represents a purely cyclonic vortex. In WBAR and in contrast to VICBAR, r_m^* corresponds with 0.8 r_m and r_i^* $(=1.5r_i)$ represents the radius where the tangential wind speed has decayed to an ordinary value of 5 m s^{-1}, indistinguishable from the background flow. Note also that the value of 5 m s^{-1} is identical to the corresponding value used in VICBAR (cf. DeMaria et al. 1992, p. 1635).

In order to retain as much information as possible in the initial fields of the numerical model, $\mathbf{F}^{BS}$ is merged smoothly with $\mathbf{F}^{VS}$ at radii greater than r_m^* to produce the final synthetic symmetric vortex $\mathbf{F}^{BO}$, which is constructed so that it is equal to $\mathbf{F}^{BS}$ for $r \le r_m^*$. For $r_m^* < r \le R$, $\mathbf{F}^{BO}$ represents a smooth transition between $\mathbf{F}^{BS}$ and $\mathbf{F}^{VS}$ using $\mathbf{F}^{BO} = (1 - W)\,\mathbf{F}^{BS} + W\mathbf{F}^{VS}$, where $W = s^2 \exp(1 - s^2)$ and $s = (r - r_m^*)/(R - r_m^*)$. Figure 2a shows an example of v^{BO} and should be compared with v^{VS} in Fig. 1d. The symmetric radial wind resulting from the azimuthal analysis, u^{VS}, is relocated to (λ_c, φ_c) and represents u^{BO}.

TABLE 5b. As in Table 5a but for comparison of WBAR with VICBAR (VBAR).

Prediction time (h)			12	24	36	48	60	72
MPE (km)	VBAR		75	147	220	301	—	544
	WBAR	comp	78	129*	184*	235*	295*	360*
		0000 UTC	76	128*	181*	241*	311*	364*
		1200 UTC	80	131	188*	229*	280*	356*
SD (km)	VBAR		43	84	123	178	—	340
	WBAR		40	76	111	133	168	181
S (%)			4.3	−12.9	−16.3	−22.1	—	−33.9
N			165	153	142	130	118	107
NWB (%)			45	62	58	59	—	62

TABLE 5c. As in Table 5a but for comparison of WBAR with the GFDL model.

Prediction time (h)			12	24	36	48	60	72
MPE (km)	GFDL		75	123	172	222	—	329
	WBAR	comp	76	129	181	232	287	342
		0000 UTC	75	128	182	244	308	353
		1200 UTC	78	130	181	220	266	332
SD (km)	GFDL		44	63	81	101	—	154
	WBAR		39	76	109	137	167	179
S (%)			2.2	4.5	5.1	4.1	—	3.8
N			158	146	132	121	108	100
NWB (%)			47	47	51	50	—	43

e. Final adjustment and construction of the model initial condition

In the final step of the initialization a ''steering concept'' is applied to the NCEP global model analyses (not to the forecasts), requiring that (U, V) at (λ_c, φ_c) corresponds with the observed translation velocity $\mathbf{c}$. In the current prediction system this is achieved by interpolation of $\mathbf{F}^{EL}$, $\mathbf{F}^{ES}$, and $\mathbf{F}^{BO}$ at (λ_c, φ_c) to give the flows $\mathbf{c}^{EL}$, $\mathbf{c}^{ES}$, and $\mathbf{c}^{BO}$. Then a matching flow $\mathbf{c}^M = \mathbf{c} - \mathbf{c}^{EL} - \mathbf{c}^{ES} - \mathbf{c}^{BO}$ is computed. Using $\mathbf{c}^M$, a field $\mathbf{F}^M = (U^M, V^M)$ is constructed within a circle of radius $r^M = 3r_i$ by application of $\mathbf{F}^M = \mathbf{c}^M[1 - s^2 \exp(1 - s^2)]$ with $s = r/r^M$ and $\mathbf{F}^M = 0$ for $s > 1$ (shown by the relative vorticity distribution in Fig. 2b). Addition of $\mathbf{F}^M$ to the sum of $\mathbf{F}^E$ and $\mathbf{F}^{BO}$ yields initial wind fields $\mathbf{F}^O$ of the numerical model that are in agreement with the requirement of the steering concept. The smooth structure of $\mathbf{F}^M$ ensures that features existing in $\mathbf{F}^{ES}$ are preserved and can take effect after initialization of the numerical model. An example of $\mathbf{F}^O$ is shown by the distribution of relative vorticity in Fig. 2c and should be compared with the original field of Fig. 1a. Note that, besides a relocation and smooth implantation of a more intense vortex, the original field at large radii is mostly preserved.

f. DLM-specific initialization procedures

Early experiments carried out during the development of WBAR produced systematic biases in the track predictions of weak or moderately strong, slow or moderately fast moving storms in the Tropics (up to category 2 hurricanes with $v_m < 50$ m s^{-1}; $|\mathbf{c}| < 10$ m s^{-1}; $\varphi_c < 24$°N). Similar systematic biases were found in the track predictions of VICBAR, while those of three-dimensional models (GFDL, UKMO, and NCEP) showed no such biases. For example, the northwestward track of Tropical Storm Gustav in 1996 (cf. Fig. 6d and its discussion in section 5) was well predicted by all baroclinic models and CLIPER, while VICBAR and WBAR predicted northward motion. These differences between barotropic and baroclinic models imply that predefined 850–200-hPa DLM fields (cf. DeMaria et al. 1992, their section 3b) may be unsuitable for the track prediction of storms with the characteristics listed above. It is likely that the track biases in the case of weaker and relatively shallow storms are caused by upper-level features in the vicinity of a storm or by upper-level remnants of vertically tilted vortices in the NCEP global model analyses and forecasts that are projected onto the DLM. In the real atmosphere and in baroclinic models, they may have only a minor influence on motion. Therefore, a storm-dependent construction of the DLM is called for in barotropic track prediction.

In order to remove or at least to weaken the influence of upper-level features in the predefined DLMs and to reduce WBARs systematic track biases, the following preliminary strategy has been applied to the NCEP global model analyses and forecasts: after the removal of the resolved vortex by the azimuthal analysis (section 3c), all wind patterns associated with isolated, quasi-circular distributions of positive relative vorticity are removed from the NCEP global model fields within a circle of 1200-km radius relative to (λ_m, φ_m). The elimination of these patterns follows the method described in sections 3b and 3c. Application of this simple ap-

TABLE 5d. As in Table 5a but for comparison of WBAR with the NHC forecasts (OFCL).

Prediction time (h)			12	24	36	48	60	72
MPE (km)	OFCL		70	129	181	223	—	339
	WBAR	comp	72	118	164	202	252	299
		0000 UTC	73	117	169	213	269	318
		1200 UTC	72	118	159	192	235	281
SD (km)	OFCL		42	61	89	123	—	157
	WBAR		36	65	94	114	148	156
S %			2.8	−8.7	−9.2	−9.2	—	−11.9
N			129	120	111	102	93	85
NWB (%)			45	56	57	56	—	60

TABLE 6. MPEs in km at all prediction times, computed separately for each storm of the 1996 hurricane season. The number of cases used to compute the MPEs is given by the values in parentheses and corresponds with the number of available VICBAR forecasts (except at 60 h where no VICBAR forecasts were available).

Storm	12 h	24 h	36 h	48 h	60 h	72 h
Arthur	53 (5)	115 (5)	186 (4)	183 (3)	230 (2)	155 (1)
Bertha	67 (16)	98 (15)	156 (14)	194 (13)	256 (12)	352 (11)
Cesar	86 (4)	161 (3)	162 (2)	132 (1)	—	—
Dolly	63 (7)	76 (6)	59 (5)	84 (4)	74 (3)	137 (2)
Edouard	59 (24)	98 (23)	131 (22)	161 (21)	202 (20)	239 (19)
Fran	64 (24)	109 (23)	167 (22)	211 (21)	277 (20)	359 (19)
Gustav	101 (9)	169 (8)	235 (7)	335 (6)	408 (5)	482 (4)
Hortense	66 (19)	89 (18)	136 (17)	183 (16)	264 (15)	354 (14)
Isidore	74 (12)	118 (11)	162 (11)	234 (10)	266 (9)	237 (8)
Josephine	126 (6)	197 (5)	377 (4)	706 (3)	1069 (2)	1673 (1)
Kyle	14 (1)	—	—	—	—	—
Lili	96 (23)	159 (22)	217 (21)	225 (20)	252 (19)	268 (18)
Marco	119 (15)	236 (14)	329 (13)	439 (12)	560 (11)	754 (10)

proach leads partly to drastic decreases in position errors in the cases of storms such as Gustav with the characteristics listed in the last paragraph. However, a storm-dependent construction of DLMs from three-dimensional datasets would be preferred instead of the present, rather crude, approach.

4. Numerical model

a. Basic equations and initial conditions

The new numerical track prediction model is based on the shallow water equations, which, in a geographical coordinate system, can be written as

$$\frac{\partial U}{\partial t} = \eta V - \frac{1}{a\cos\varphi}\frac{\partial E}{\partial \lambda}, \tag{4.1}$$

$$\frac{\partial V}{\partial t} = -\eta U - \frac{1}{a}\frac{\partial E}{\partial \varphi}, \tag{4.2}$$

$$\frac{\partial h}{\partial t} = -\frac{1}{a\cos\varphi} \times \left[\frac{\partial}{\partial \lambda}(hU) + \cos\varphi\frac{\partial}{\partial \varphi}(hV) - hV\sin\varphi\right], \tag{4.3}$$

where E is the total energy, given by

$$E = gh + \frac{1}{2}(U^2 + V^2), \tag{4.4}$$

and the absolute vorticity η is defined as

$$\eta = \frac{1}{a\cos\varphi}\left[\frac{\partial V}{\partial \lambda} - \cos\varphi\frac{\partial U}{\partial \varphi} + U\sin\varphi\right] + 2\Omega\sin\varphi. \tag{4.5}$$

In addition to the abbreviations used earlier, t is time, h is geopotential height, a is the radius of the earth, Ω is the rotation frequency of the earth, and g is the gravity acceleration. Latitude and longitude are defined in radians. All equations are discretized using finite differences of second-order accuracy, with horizontal grid sizes $\Delta\lambda$ and $\Delta\varphi$ equal to 0.5° (cf. Table 1 for comparison with VICBAR) and the integration domain corresponds with that of the NCEP global model analyses and forecasts (cf. section 2).

The individual contributions (U^O, V^O) and (U^{BO}, V^{BO}) of the postanalysis of the NCEP global model analyses at $t = t_0$ and at $t = t_0 - 12$ h and forecasts are interpolated separately to the model grid using exactly the same interpolation methods as in the initialization procedure. Note that (U^{BO}, V^{BO}) are zero in the case of the NCEP global model forecasts. The corresponding distributions of geopotential height deviation are computed using a nonlinear divergence equation in a geographical coordinate system without a tendency term of the form

$$\begin{aligned} ga^2\cos^2\varphi\nabla^2 h = {} & -U\frac{\partial^2 U}{\partial \lambda^2} - V\cos^2\varphi\frac{\partial^2 V}{\partial \varphi^2} - \cos\varphi\left[V\frac{\partial^2 U}{\partial \lambda\partial \varphi} + U\frac{\partial^2 V}{\partial \lambda\partial \varphi}\right] \\ & - \frac{\partial U}{\partial \lambda}\left[\frac{\partial U}{\partial \lambda} - V\sin\varphi\right] \\ & - \frac{\partial V}{\partial \lambda}\left[2\cos\varphi\frac{\partial U}{\partial \varphi} - U\sin\varphi - fa\cos\varphi\right] \\ & - \cos\varphi\frac{\partial U}{\partial \varphi}[2U\sin\varphi + fa\cos\varphi] \\ & - \cos\varphi\frac{\partial V}{\partial \varphi}\left[\cos\varphi\frac{\partial V}{\partial \varphi} - V\sin\varphi\right] \\ & - aU\cos\varphi\left[\frac{U\cos\varphi}{a} - f\sin\varphi + \cos\varphi\frac{\partial f}{\partial \varphi}\right] \end{aligned} \tag{4.6}$$

with $f = 2\Omega\sin\varphi$. The second-order finite-difference representation of Eq. (4.6) is solved for Dirichlet boundary conditions with a method described in Swarztrauber and Sweet (1975, their section VII, 115–131). The boundary values of h on the model grid are computed by birational interpolation as before. The final geopo-

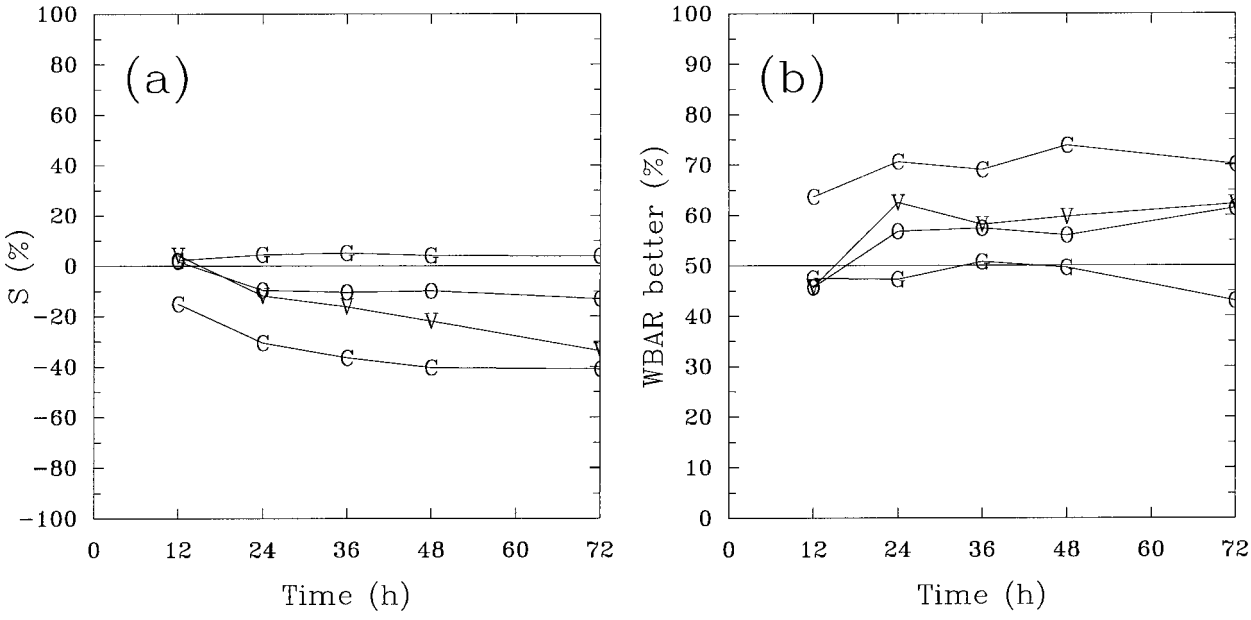

FIG. 4. (a) Skill S in % vs prediction times of WBAR relative to CLIPER (C), VICBAR (V), the GFDL model (G), and the official NHC forecasts (O) at 12-, 24-, 36-, 48-, and 72-h prediction time. Negative values represent positive skill. (b) As in (a) but for percentage of superior track guidance vs prediction times of WBAR relative to the models listed above. Note again that the 60-h positions of the other models and the official forecasts were not available.

tential height is obtained by adding a scale height H_0 of 750 m to the solution of Eq. (4.6). Note that H_0 is exactly the same as in VICBAR (Table 1; cf. DeMaria et al. 1992, p. 1633). If h is zero or negative somewhere in the integration domain, increments Δh of 100 m are added until h is positive everywhere. All equations used for the track prediction are scaled using a velocity scale U_0, defined as the absolute maximum of (U, V) in the integration domain, a length scale L_0 of 200 km and the scale height H_0. Time is nondimensionalized using an advective timescale L_0/U_0.

b. Time-dependent boundary conditions and time integration

At each grid point in the integration domain, the postanalyses of NCEP global model analyses at $t = t_0 - 12$ and $t = t_0$ h and forecasts until $t = t_0 + 72$ h can be computed at any time t using the coefficients of a one-dimensional rational interpolation method (Späth 1990). The temporal boundary conditions at $t = t_0 - 12$ and $t = t_0 + 72$ h are calculated using first-order finite differences. In this way, the postanalyses of the NCEP global model analyses and forecasts form continuous time-dependent boundary conditions $(U, V, h)^B$ that can be retrieved after every time step.

The prognostic equations (4.1)–(4.3) are integrated with respect to time in a circular vortex-relative domain of radius R_B, centered on the current predicted storm position. Between the radius $R_A < R_B$ and R_B, the barotropic forecasts are adjusted after every time step to the time-dependent boundary conditions by $(U, V, h) = (U, V, h)^{\text{old}}(1 - Q) + Q(U, V, h)^B$ with $Q = 0.5[1 - \cos(\pi S)]$, $S = (r - R_A)/(R_B - R_A)$ and $R_A \le r \le R_B$ [cf. DeMaria et al. 1992, their Eq. (3.5)]. Based on a large number of sensitivity tests using all 1996 storm cases and on the assumption that relatively fast-moving, stronger storms in higher latitudes ($|\mathbf{c}| \ge 10$ m s^{-1}; $v_m \ge 30$ m s^{-1}; $\varphi_c \ge 24°$N) may be affected by the surrounding flow to a lesser extent than slower-moving, weaker storms in the Tropics, the values of R_A and R_B are chosen storm dependent: For the above values of $|\mathbf{c}|$, v_m, and φ_c, R_A and R_B are set to 1000 and 3000 km, while for smaller values of $|\mathbf{c}|$, v_m, and φ_c, R_A and R_B are set to $2r_i$ and 6 r_i, respectively. This allows a greater impact of the baroclinic evolution on the barotropic development in the vicinity of slow and weak storms in the Tropics. The vortex-relative domain is relocated every hour and centered either on the current storm position in the model or on a position that allows the circular domain to lie completely inside the NCEP global model domain.

The model time steps are variable and determined automatically by evaluation of the Courant–Friedrich–Levy criterion using the current fields of (U, V, h). For reasons of computational stability, the time steps are multiplied by a safety factor of 0.3. An Euler forward step and a third-order Adams–Bashforth step are used for the first two time steps, while all other time steps are Adams–Bashforth steps of third-order accuracy as described in Durran (1991). After each time step, the new predicted storm position is computed by locating

the maximum or minimum of relative vorticity, depending on the hemisphere, in a way similar to that explained in section 3b.

At 1-hourly intervals, all dependent variables are subjected to a smoother–desmoother procedure, designed to remove 2-Δ waves and to damp short waves but retain long waves. This procedure is based on the work of Shapiro (1970), but applied using the same formulation as in the Pennsylvania State University–National Center for Atmospheric Research fifth-generation Mesoscale Model (Grell et al. 1994, p. 27f).

5. Forecast results

This section focuses on a statistical analysis of the results produced by the research version of WBAR in 1996 on the basis of the verification and comparison datasets listed in section 2. In particular, the results obtained with WBAR are compared with those of CLIPER in 166 cases, VICBAR in 165 cases, the GFDL model in 158 cases, and the official NHC forecasts in 129 cases. The reason for this choice is that a comparison with CLIPER can be seen as a benchmark test of WBAR, while VICBAR represents the best barotropic model available in 1996 and the GFDL model and the NHC produced on average the best track guidance in 1996 in comparison with all other models (including the UKMO model).

Serial correlation of successive track predictions (Neumann et al. 1977) was tested using the same procedure as described in Aberson and DeMaria (1994, their p. 2806 and appendix B). Following the method described by the above authors, track predictions with the new model become uncorrelated for separation times of successive forecasts of 13.5, 15.0, 15.4, 16.6, 15.8, and 15.6 h (mean 15.3 h) at prediction times 12, 24, 36, 48, 60, and 72 h, respectively. These values do not differ much from the true separation time of 12 h (cf. section 2). As a consequence, the differences in mean position errors (defined in the appendix and henceforth referred to as MPE) between two distinct subsets of track predictions at base times 0000 and 1200 UTC and the complete set of track predictions are relatively small, as shown in the first rows of Tables 5a–d for homogeneous comparisons with CLIPER, VICBAR, the GFDL model, and the NHC forecasts, respectively. Tables 5a–d show also the results of a paired Student's *t*-test (Press et al. 1986, p. 467f), carried out to determine the statistical significance of the differences between the MPEs of WBAR and the other models. The *t* test is based on the null hypothesis that the differences between the MPEs of WBAR and those of the other models are not significantly different from zero. Statistical significance is tested at the 95% level and marked by stars in the Tables 5a–d. The MPEs of WBAR are found to differ significantly from those of CLIPER at all prediction times and from those of VICBAR at all prediction times except 12 h. As expected (cf. also Fig. 3, showing the MPEs of WBAR in comparison with the other models), the MPEs of WBAR and the GFDL model and the NHC forecasts are not significantly different.

a. General performance of the new track prediction system in 1996

Figure 3 shows homogeneous comparisons of the MPEs of WBAR with those of CLIPER, VICBAR, the GFDL model, and the official forecasts of the NHC. The corresponding numerical values are given in the first rows of Tables 5a–d (headed by ''comp''). Note that the particular MPEs differ as a consequence of different numbers N of available model forecasts (shown in the fourth rows of Tables 5a–d). The new system produces smaller MPEs than CLIPER at all analysis times (Fig. 3a). On average, both VICBAR (Fig. 3b) and the official NHC forecasts (Fig. 3d) provide slightly better track guidance at 12 h, while at all other prediction times WBAR performs better. Figure 3c shows, in agreement with the *t* test discussed earlier, that the results of WBAR and the GFDL model are very similar, but WBAR has slightly higher MPEs than the GFDL model at all prediction times.

The 66.6% levels of the standard deviation of the MPEs produced by WBAR are much smaller than those of CLIPER and VICBAR and comparable to those of the GFDL model and the official forecasts. This is indicated by the shaded areas in Fig. 3 (the numerical values are given in the second rows of Tables 5a–d, respectively). The reason for the differences in standard deviations between VICBAR and CLIPER and WBAR lies in a drastic reduction of the number of large position errors with the new system. For example, of 108 CLIPER forecasts at 72-h prediction time in 1996, position errors exceeded 500 km in 54 and 1000 km in 19 cases. VICBAR produced 42 position errors over 500 km and 16 position errors over 1000 km for a total number of 107 forecasts at 72-h prediction time in the same year. In the case of WBAR, the corresponding position errors exceed 500 km in 22 cases and 1000 km in 3 cases for a total number of 108 forecasts at 72-h prediction time.

The MPEs discussed above can be expressed in terms of skill *S* (defined in the appendix) of WBAR relative to the other models. Figure 4a (the numerical values are given in the third rows of Tables 5a–d) shows that the new system has an approximately constant positive skill (negative relative MPEs) of more than 30% relative to CLIPER after 12 h of prediction time. Relative to VICBAR, the skill of the new system increases with time from a slightly negative value at 12 h to 34% at 72 h. Moreover, the new system is comparable in skill even relative to the 1996 NHC official forecasts and the GFDL model after 12 h of prediction time. Additionally, Fig. 4b shows the percentage of better performance of WBAR in comparison with the other models at any given prediction time. Averaged over all available prediction times, WBAR produces better track guidance

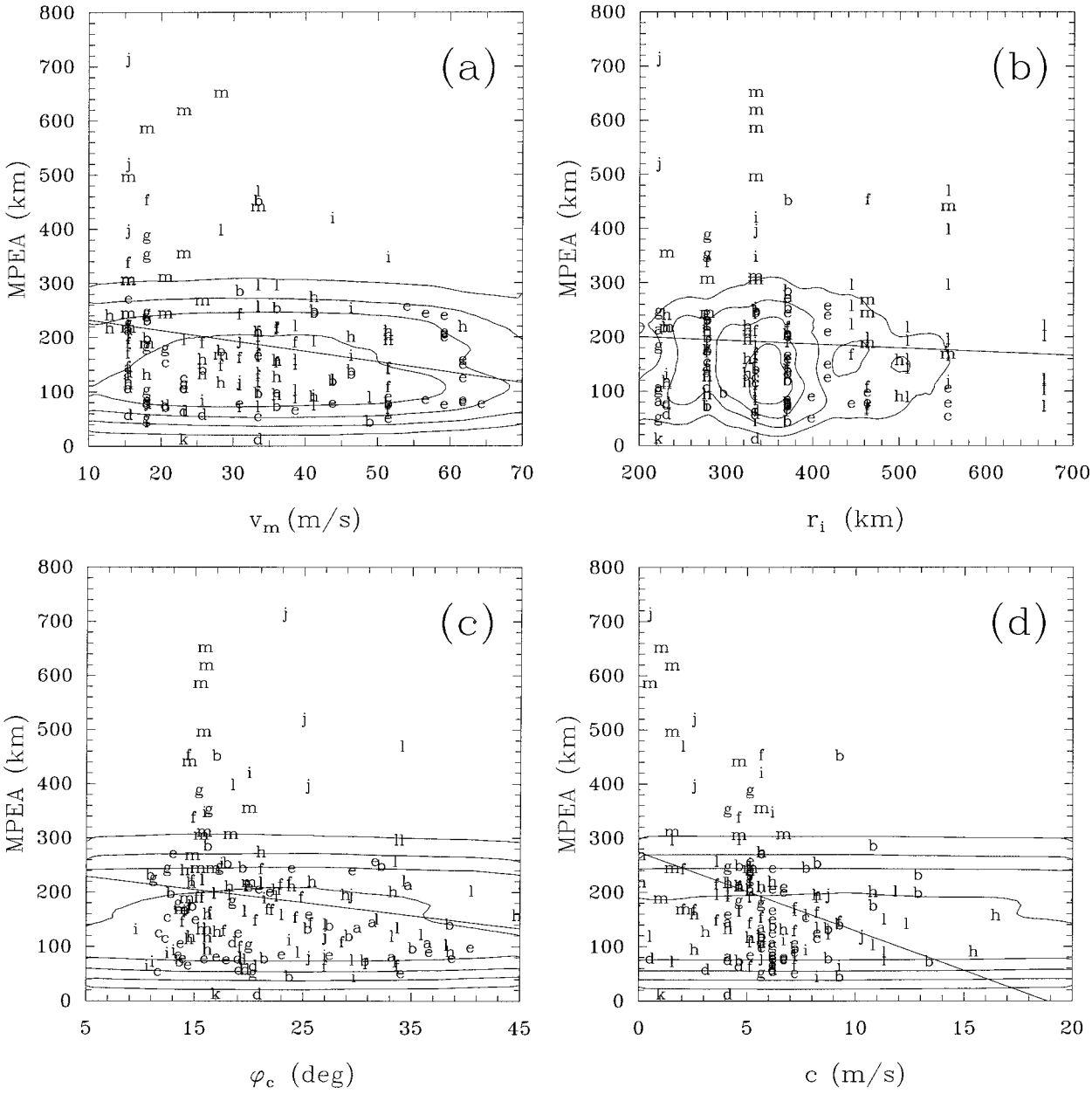

FIG. 5. Scatter diagrams of the MPEAs in km ($N = 1$ in the appendix) of WBAR at all base dates/times vs (a) v_m in m s^{-1}, (b) r_i in km, (c) φ_c in °, (d) c in m s^{-1}, and (e) c_d in ° counterclockwise from east at the base dates/times as provided by the TC advisories. The straight lines define linear least square fits and the contours represent an approximate density distribution of all MPEAs. The letters *a*, . . ., *m* represent the 1996 storm names.

than CLIPER in 69%, VICBAR in 57%, the official forecasts in 55%, and the GFDL model in about 48% of all cases examined. The corresponding values at each prediction time are listed in Tables 5a–d.

b. Storm-dependent performance and performance variability in 1996

The 1996 Atlantic hurricane season (cf. Table 2) forms an ideal testbed for the development of a new track prediction model and for sensitivity studies because of the large number of storms and their variety in location ($10° \le \varphi_c \le 45°$), strength ($13 \le v_m \le 64$ m s^{-1}), size ($220 \le r_i \le 670$ km), translation speed ($0 \le c \le 17$ m s^{-1}) and evolution. Among the 13 storms in 1996 (cf. Pasch and Avila 1999), Cape Verde storms (Bertha, Edouard, Fran, and Isidore) are found as well as storms forming or developing in the Caribbean Sea and the Gulf of Mexico (Cesar, Josephine, Kyle, Lili, and Marco) or along the U.S. eastern coastline (Arthur).

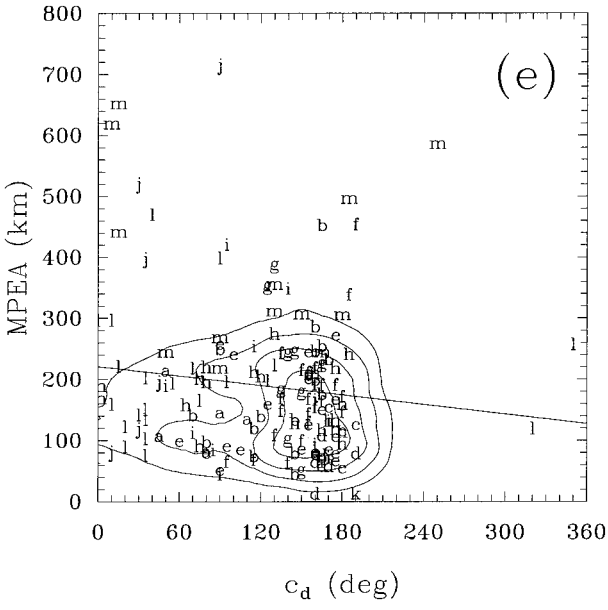

FIG. 5. (*Continued*)

The 1996 Atlantic hurricane season included four tropical storms (Arthur, Gustav, Josephine, and Kyle), nine hurricanes, and 10 storms that affected land. Storm motion included cases of straight-moving storms (Bertha, Edouard, or Fran) as well as recurving storms (Bertha, Edouard, Hortense, or Isidore) or erratically moving storms (Josephine, Lili, or Marco). The broad spectrum of storms in 1996 also leads to the expectation that the initialization and model parameters discussed in sections 3 and 4 are valid also for storms occurring during other seasons or in other regions where tropical cyclones occur.

The main storm-dependent characteristics of WBAR and its storm-by-storm performance are documented in Table 6 and the scatter diagrams of Fig. 5. They can be summarized as follows: as in the case of VICBAR (cf. Aberson and DeMaria 1994), the new system seems to perform better in cases of stronger storms. However, Fig. 5a shows that the average trend, defined by the straight line, may not be a satisfactory estimate for the model performance: the new system performs well also in many cases of relatively weak and possibly shallow storms or storms of moderate strength in spite of the expectation that deep 850–200-hPa DLMs may not adequately represent atmospheric features governing the motion of such storms. The WBAR model seems to produce better track guidance in cases of storms with influence radii smaller than 400 km, as shown in Fig. 5b. Figure 5c shows the dependence of the track forecasts on the initial storm latitude. On average, storm tracks at higher latitudes are predicted better than storms at low latitudes, although WBAR performs relatively well at all latitudes. Perhaps the only storm parameter with a significant influence on the performance of WBAR is the translation speed (Fig. 5d). Position errors decrease with increasing speed of motion of storms. This is possibly a consequence of the adjustment of the initial wind fields at (λ_c, φ_c) to the observed translation velocity (cf. section 3e), which supports a persistence of the initial direction of motion during the forecast, and the experience that many fast-moving storms tend to move steadily in one direction. Finally, Fig. 5e shows that WBAR performs better in cases of westward or northwestward-moving storms than in cases of eastward- or northward-moving storms.

More subjective interpretations of the forecast results of WBAR indicate a lack of skill relative to the other models in cases of relatively weak high-latitude storms such as Arthur (Fig. 6a) interacting with midlatitude weather systems. Midlatitude systems may form a strong azimuthal wavenumber one asymmetry relative to the storm and affect its motion. Consequently, their partial or total elimination by the procedure described in section 3c may have a negative effect on track prediction. In contrast, recurving and straight-moving storms are often predicted with satisfactory precision in comparison with the other models, as the examples of Bertha (Fig. 6b) and Edouard (Fig. 6c) show. This subjective impression is confirmed by the better model performance in cases of westward or northwestward motion, as shown in Fig. 5e, which often occurs prior to the period of recurvature. Systematical large position errors over periods of several subsequent base dates/times occur mainly in the case of relatively small, slow-moving, and weak storms (cf. Figs. 5a, 5b, and 5d) like Gustav (Fig. 6d), Josephine (not shown), and Marco (Fig. 6f). As indicated in Table 6, WBAR has quite large 72-h MPEs of 482, 1673, and 754 km in these three cases. However, the corresponding values of VICBAR are even larger (cf., e.g., Figs. 6d and 6f). The unsatisfactory performance of VICBAR and WBAR in comparison with all other models may be a consequence of the projection of upper-level features on to the 850–200-hPa DLMs, leading to an unrealistically strong influence of these features on the motion of the three weak and possibly shallow storms. However, the satisfactory performance of WBAR in many other cases of weak, small, and slow-moving storms (cf. also Fig. 5a, 5b, and 5d) implies that the above arguments cannot be generalized. Further experiments are required to test the impact of storm-dependent DLMs on the performance of barotropic track prediction models in the case of weak storms. Finally, the position errors of WBAR become relatively large later in the season (e.g., Josephine and Marco; cf. Table 6 and Fig. 6f), as is the case with VICBAR (Aberson and DeMaria 1994). However, for example, the 72-h forecasts of WBAR in the case of the late-season Hurricane Lili (Fig. 6e; cf. also Table 6) were found to be far superior to that of all other models. In particular, the period of erratic motion after 1200 UTC 21 October 1996 was captured very well and shows the potential of WBAR to predict even late-seasonal storms with satisfactory precision.

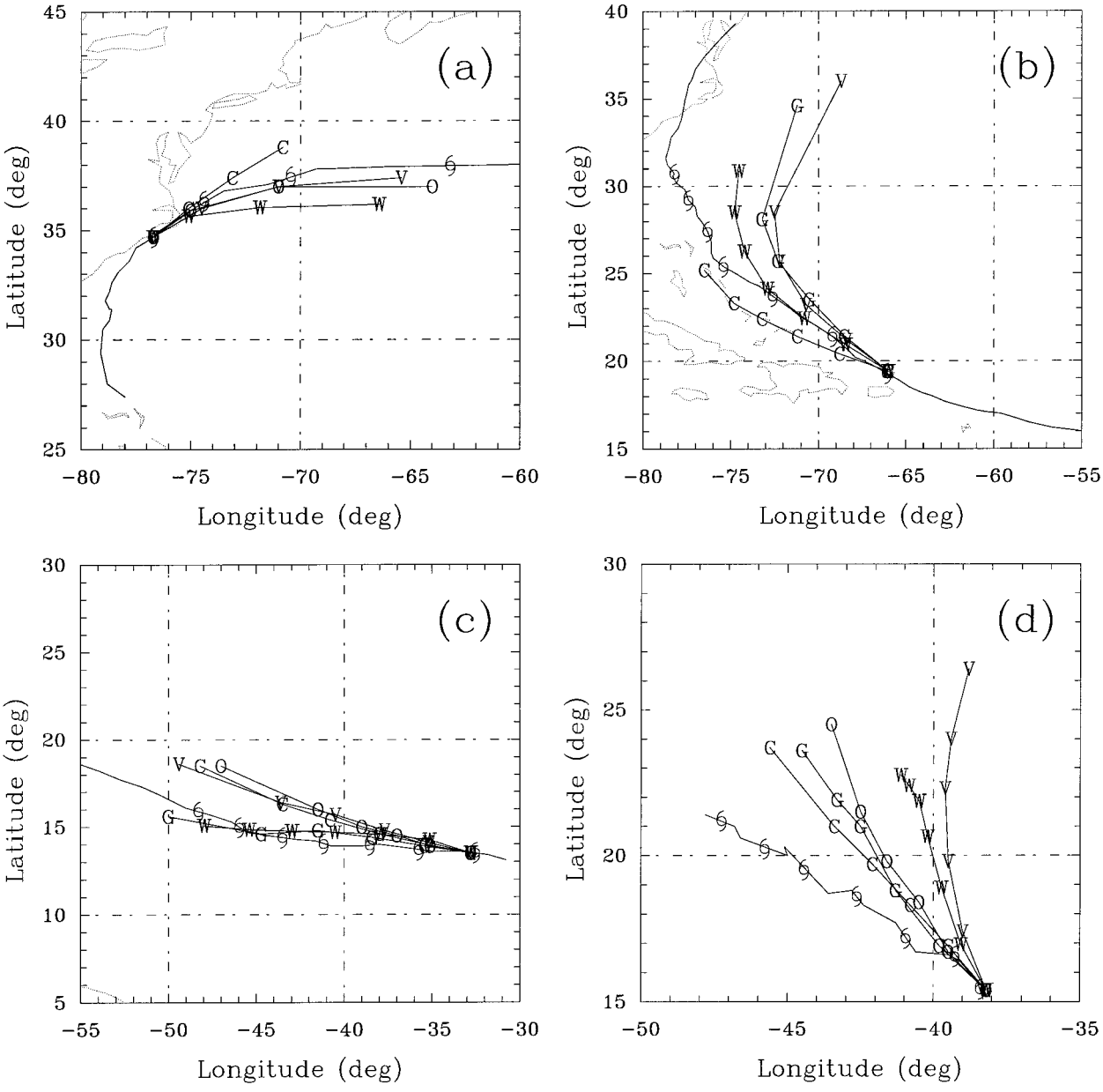

FIG. 6. Selected forecasts of WBAR (W), CLIPER (C), VICBAR (V), the GFDL model (G), and the NHC (O). The original track is shown by the hurricane symbols. Positions are given at 12-hourly intervals: (a) Arthur, 0000 UTC 20 Jun 1996; (b) Bertha, 0000 UTC 9 July 1996; (c) Edouard, 1200 UTC 22 Aug 1996; (d) Gustav, 0000 UTC 30 Aug 1996; (e) Lili, 1200 UTC 20 Oct 1996; and (f) Marco, 1200 UTC 22 Nov 1996. Continents are outlined in dotted contours. Note that the 60-h positions of CLIPER, VICBAR, the GFDL model, and the NHC forecasts were not available and are not shown.

It is of interest to examine the storm-dependent skill and reliability of WBAR relative to other numerical models. Therefore, Figs. 7 and 8 show scatter diagrams of the mean skill at all prediction times SA (defined in the appendix; note that negative values represent positive skill) of all track predictions relative to VICBAR and the GFDL model, respectively. On average, WBAR performs better than VICBAR in cases of weak or moderately strong storms ($18 \leq v_m \leq 30$ m s^{-1}; Fig. 7a) at lower latitudes ($13° \leq \varphi_c \leq 25°$; Fig. 7c) that move to the west or northwest ($120° \leq c_d \leq 180°$; Fig. 7e). VICBAR seems to perform slightly better in cases of stronger storms ($33 \leq v_m \leq 50$ m s^{-1}; Fig. 7a) at higher latitudes ($\varphi_c \geq 25°$; Fig. 7c). No significant differences in the performance of VICBAR and WBAR can be found in terms of the influence radius (Fig. 7b) and the translation speed (Fig. 7d), although the linear trend indicates a slightly better performance of the new system in both cases. Comparison with the GFDL model (Fig. 8) leads to similar skill characteristics of WBAR

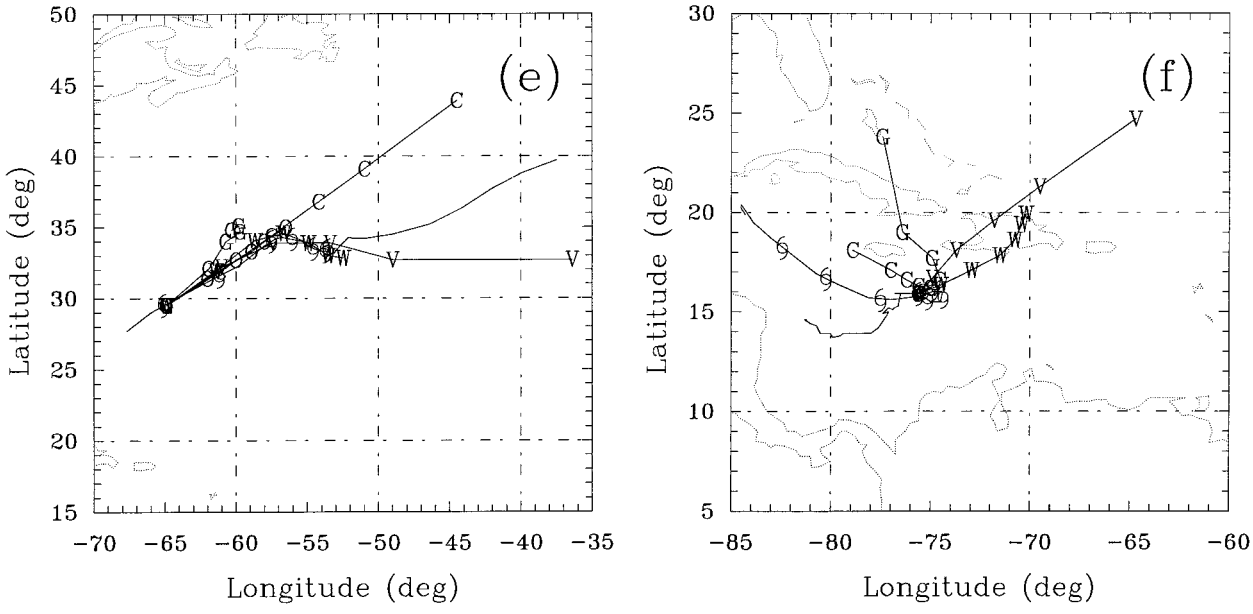

FIG. 6. (*Continued*)

as described above, but with smaller differences between model performances. The new system performs slightly better than the GFDL model in cases of storms at lower latitudes ($13° \leq \varphi_c \leq 25°$; Fig. 8c) that move to the west or northwest ($120° \leq c_d \leq 180°$; Fig. 8e). The performance relative to maximum wind speed (Fig. 8a), influence radius (Fig. 8b), and translation speed (Fig. 8d) seems to be in balance, with slightly less skill of the new system in cases of medium-sized storms ($300 \leq r_i \leq 400$ km; Fig. 8b) and slightly more skill in cases of faster-moving storms ($c \geq 5$ m s^{-1}). Comparison with CLIPER (not shown) indicates a positive skill of the new track prediction system that is nearly independent of the storm parameters, with a few exceptions: CLIPER performs better than WBAR in the case of Hurricane Edouard during its period of highest intensity and in the cases of Gustav, Josephine, and Marco, possibly for the same reasons as discussed earlier in this section.

A storm-by-storm comparison of the MPE of all prediction times (MPEA, defined in the appendix) of WBAR with VICBAR (Fig. 9a) shows a high correlation in storm-by-storm performance, possibly a consequence of using the same basic datasets. However, Fig. 9a shows also that the MPEAs of the new system are smaller than those of VICBAR in all cases except Arthur, Fran, and Hortense. No systematic explanation for the lack of skill of WBAR relative to VICBAR in these three cases has been found. More interesting though are the differences in storm-by-storm performance of the GFDL model and WBAR, shown in Fig. 9b. The two models perform nearly equally well in all cases except for four storms: Dolly, Gustav, Josephine, and Marco. For the latter three cases, the track predictions of WBAR showed the systematical large position errors discussed earlier in this section. Moreover, these three weak storms account almost exclusively for the lack of skill of WBAR relative to the GFDL model. For unknown reasons, the GFDL model shows a lack of skill versus WBAR in the case of the relatively weak storm Dolly. Without Dolly, Gustav, Josephine, and Marco, the GFDL model and WBAR produce MPEs of 69, 113, 162, 215, and 305 km and 69, 112, 161, 200, and 302 km after 12, 24, 36, 48, and 72 h of prediction time, respectively (Fig. 9c; cf. also the original values given in Table 5c). As discussed earlier, this result suggests that barotropic track prediction may be improved by a storm-dependent construction of DLMs.

c. Unsuccessful initialization methods

This section focuses on variations of the postanalysis method that did not lead to a satisfactory quality of track prediction. Of the large number of sensitivity experiments carried out for the present study, only the more important different approaches are listed and discussed below. It should be noted that the term ''unsuccessful'' in the heading refers to the MPE of all cases investigated. In particular cases or even in sequences of cases, unsuccessful initialization methods may produce superior track forecasts in comparison with the current method, but no consistent reduction of the MPE. Furthermore, it is important to note that, on average, all of the approaches listed in this section produced better overall track guidance than VICBAR in 1996.

First, an analysis of the wind components is found to be preferable to an analysis of relative vorticity and divergence fields for the following reasons: the analysis

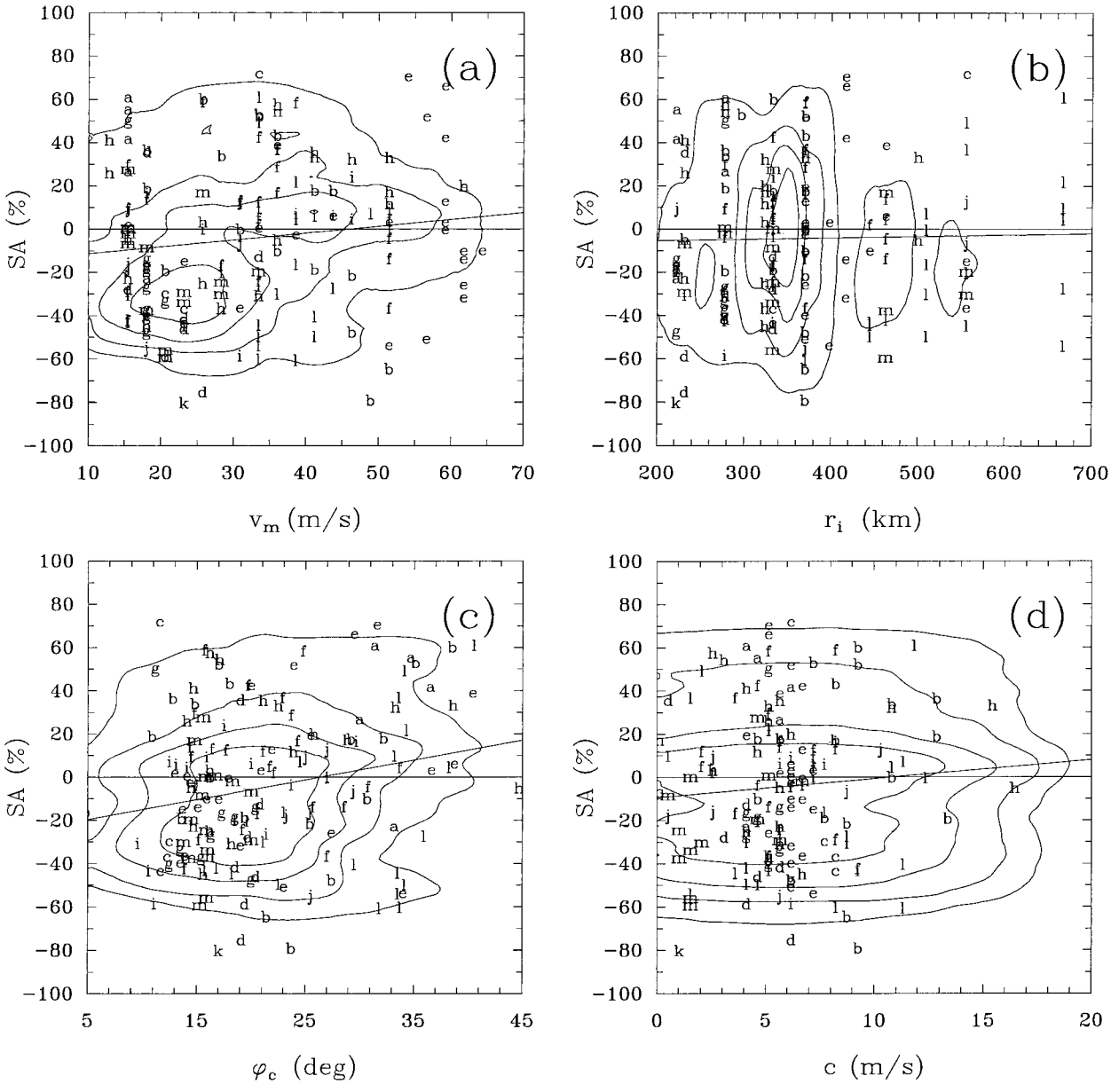

FIG. 7. Scatter diagrams of the mean skill of all prediction times (SA, defined in the appendix) in % of WBAR relative to VICBAR at all base dates/times vs (a) v_m in m s^{-1}, (b) r_i in km, (c) φ_c in °, (d) c in m s^{-1}, and (e) c_d in ° counterclockwise from east at the base dates/times as provided by the TC advisories. The straight lines define least square fits and the contours represent an approximate density distribution of all SAs. The letters *a*, . . ., m represent the storm names.

of vorticity and divergence neglects an irrotational nondivergent (harmonic) wind field that is not necessarily small in magnitude compared with the rotational and divergent wind contributions. Furthermore, the elliptic equations used to compute the streamfunction and velocity potential from vorticity and divergence depend strongly on the boundary conditions and do not produce unique solutions of the harmonic wind. Preliminary sensitivity experiments showed that the track predictions starting from analyzed vorticity and divergence fields resulted in much larger MPEs than those starting with wind field analyses. However, these results are not conclusive and further tests are required to confirm these preliminary findings.

Several modifications of the currently used synthetic symmetric tangential wind profile have been tested. As in DeMaria (1987, his section 4c), track forecasts were found to be insensitive to changes in v_m. High values of v_m lead to the occurrence of gravity waves in the current version of WBAR during the first few hours of

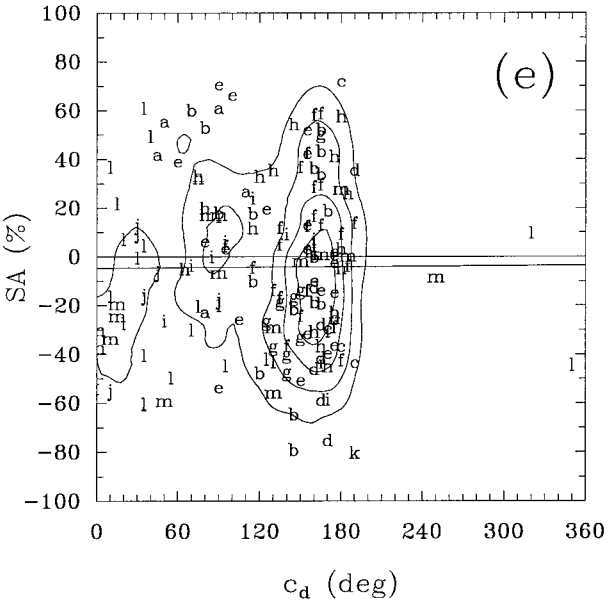

FIG. 7. (*Continued*)

time integration, but have little effect on the track predictions as such. This was examined by successively decreasing the value of v_m during the construction of the synthetic vortex, which led to decreased gravity wave activity at early hours but insignificant changes of the predicted track. As expected from earlier studies (e.g., DeMaria 1985), successive changes of the outer structure of $\mathbf{F}^{BO}$ (by variation of the tangential wind speed at r_i^*; cf. section 3d) lead to a large spread of the predicted tracks. However, no systematic relation between the changes in outer wind structure and the predicted tracks could be detected. The implementation of synthetic vortices with zero integrated relative angular momentum, as suggested by DeMaria (1987), did not improve the performance of the track prediction system. One possible reason for this result may be that in many cases the blending of $\mathbf{F}^{BS}$ and $\mathbf{F}^{VS}$ results in synthetic vortices with anticyclonic tangential winds at larger radii and thus a reduced value of integrated relative angular momentum in comparison with that of the purely cyclonic vortex $\mathbf{F}^{BS}$.

A number of different methods for the adjustment of the initial wind fields at (λ_c, φ_c) to the observed motion were tested and found to produce unsatisfactory results in comparison with the current method. The following list summarizes some of the more important approaches.

1) During a cold start, the model is initialized with the original global model analysis and forecasts. Only the symmetric vortex computed during the postanalysis (cf. section 3c) is replaced by a synthetic symmetric vortex (cf. section 3d). Tests show that the position errors become relatively large after short periods of time, often already after 12 h of prediction time. In all probability, the large position errors occur as a result of the absence of a method adjusting the initial storm motion in the model to the observed storm motion. In most of the cases examined, the initial induced flow across the vortex center (as defined in section 3e) differs strongly from the observed translation velocity, leading to a motion of the model storm that deviates from the observed motion almost instantaneously. This result points to the importance of an adjustment of the initial wind fields with regard to barotropic track prediction.
2) A direct adjustment of $\mathbf{F}^{EL}$ to $\mathbf{c}^M = \mathbf{c} - \mathbf{c}^{ES} - \mathbf{c}^{VS}$ by computation of $(1 - W)\,\mathbf{F}^{EL} + W\mathbf{c}^M$ with $W = 1 - s^2 \exp(1 - s^2)$, $s = r/r^M$, and $r^M = 1500$ km (cf. section 3e) appears to smooth $\mathbf{F}^{EL}$ too strongly in the vicinity of the vortex and leads to a slight degradation of the average forecast quality. However, the above approach produces better track guidance than the current approach in cases of very strong storms with v_m greater than 50 m s^{-1} (e.g., Edouard). This is possibly a result of the strong smoothing, which increases the model storm's tendency to follow the observed motion during early hours of the forecast.
3) A direct adjustment of $\mathbf{F}^{ES}$ in a way equivalent to that discussed under approach 2 above leads to an improvement in a few cases of straight-moving storms, but to a degradation of performance in nearly all other cases. The reasons for the unsatisfactory performance are possibly the same as those discussed under approach 2, but with a stronger effect due to the weakening of features of smaller horizontal scale in $\mathbf{F}^{ES}$. The better performance of the current approach, where $\mathbf{F}^{ES}$ is modified very little, points out the relative importance of smaller-scale features with regard to track prediction and also the high quality of the datasets provided by NCEP.
4) The implementation of vortex asymmetries [exactly in the same way as described in Davidson and Weber (2000, their section 3 and appendix)] produces excellent track predictions in some cases of recurving storms (e.g., Bertha after 1200 UTC 10 Jul), but leads to too early and too fast recurvatures in cases of straight-moving storms (e.g., Bertha or Edouard before recurvature) or to recurvatures in cases of low-latitude storms (e.g., Cesar, Dolly, or Marco) otherwise. These unsatisfactory and inconsistent performance characteristics are possibly caused by the principally unpredictable and nonlinear adjustment of the arbitrary asymmetries to the symmetric vortex and its surrounding flow in the numerical model.
5) The implantation of β gyres [constructed on the basis of the analytical theory of vortex motion of Smith and Ulrich (1990), Smith (1991), and Smith and Weber (1993)] with and without postadjustment of $\mathbf{F}^{EL}$ (in a similar way as described under approach 2 above) to $\mathbf{c}^M = \mathbf{c} - \mathbf{c}^{\beta} - \mathbf{c}^{ES} - \mathbf{c}^{VS}$, where $\mathbf{c}^{\beta}$ denotes the flow induced by the β gyres, leads to a drastic increase of the MPEs and in a number of cases even

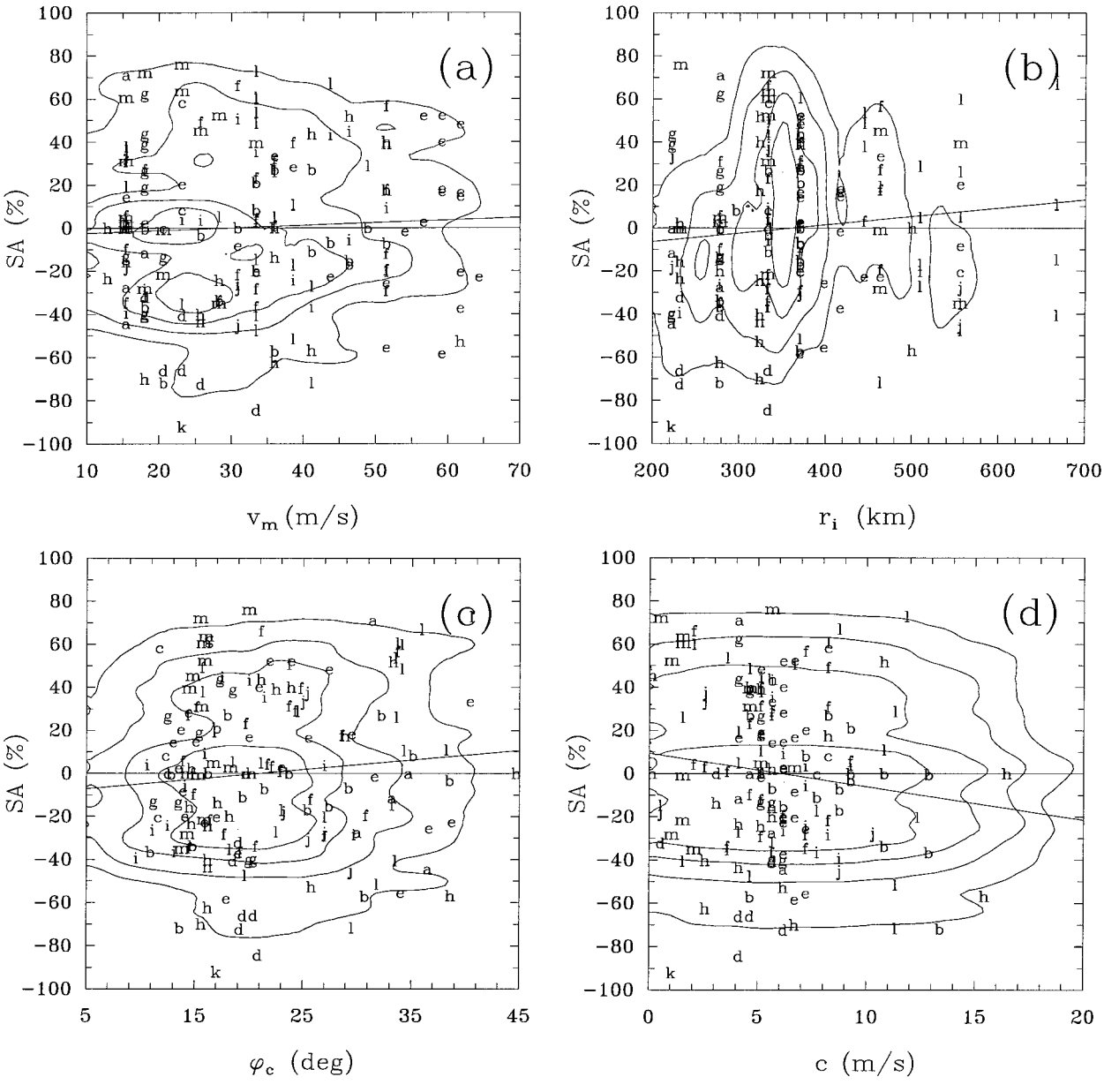

FIG. 8. As in Fig. 7 but for skill (SA) relative to the GFDL model.

to catastrophic track predictions. This points to a principal problem with the application of the barotropic theory of vortex motion (see, e.g., Fiorino and Elsberry 1989) to practical concepts of tropical cyclone track prediction: first, real tropical cyclones do not exist in a quiescent environment in which β gyres can develop undisturbed. Analyses of the predicted wind fields show that, even after a computation of the β gyres on the basis of the model representation of the initial symmetric vortex, the gyres are modified or even completely destroyed during the first hours of time integration. A balance between the symmetric vortex and the β gyres as in the framework of theoretical experiments does not exist. A systematic analysis of the corresponding track forecasts and forecast sensitivities is impossible, because the initial β gyres are modified unpredictably in response to nonlinear interaction with the particular initial condition of the numerical model, that is, the flow in which the model storm is embedded; and second, the β gyres of a vortex in a quiescent environment evolve with time, which adds the construction time of the β gyres as an arbitrary and generally unknown free parameter to the initialization procedure (cf. Ross and Kurihara 1992).

Separate computation of an ''observed'' translation

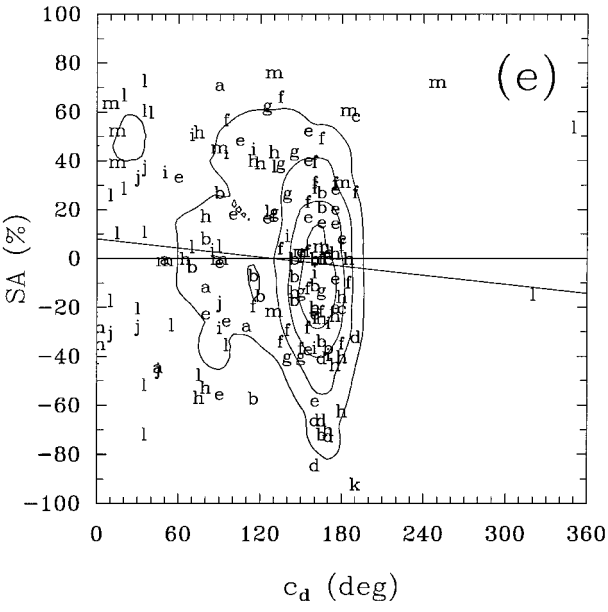

FIG. 8. (*Continued*)

velocity **c** of a given storm by fitting a second-order polynomial through the storm positions at t_0, $t_0 - 12$ h, and $t_0 - 24$ h (provided by the operational TC advisories) yields a better estimate of the true translation velocity[6] than the estimate given in the TC advisories in about 60% of all cases investigated. However, the application of this translation velocity to the current track prediction system does not lead to a decrease in MPEs and points to the superior quality of the translation velocity estimates provided by the operational TC advisories.

6. Concluding remarks

The new barotropic track prediction system WBAR, presented in this study, has been developed, optimized, and tested using a large number of storm cases of the 1996 Atlantic hurricane season. It was found capable of providing excellent track guidance for up to 72-h prediction time. This result extends the findings of DeMaria et al. (1992) and Aberson and DeMaria (1994) insofar as the common assumption that barotropic models are generally unable to produce valuable track guidance after 48 h may need some reconsideration. Based on a strategy for careful initialization, WBAR produced 72-h track predictions that were superior to all barotropic models used during the 1996 Atlantic hurricane season, including the semioperational VICBAR model. Presumably for the same reason, the 1996 track predictions of WBAR were even found to be competitive to the best models currently in operational use (for a detailed summary of WBAR's performance, see section 5). In this context it is important to note also that valuable track guidance was achieved *without* an inclusion of all possibly available information such as ODW data or satellite-derived cloud-drift winds, which are used operationally in nearly all operational models.

The broad spectrum of storms during the 1996 Atlantic season (cf. Table 2) leads to the expectation that the specific parameters used for the model initialization and the numerical model itself may prove to be valid also during different seasons or for storms occurring in different ocean basins. However, in view of a possible extension of the current research version of WBAR to an operational track prediction model in the future, we are aware that further tests, continuous checks, and possibly also modifications of the model parameters are required. To assess the general validity of the performance of WBAR, the ongoing (see below) and future tests will need to prove that WBAR has the capability to provide valuable track guidance for a wide variety of tropical cyclone events during other years or in different geographical regions. This also includes runs of WBAR from different databases.

The development of a numerical model like the one presented in this study always leaves room for improvements: 1) One such improvement might result from a storm-dependent construction of DLMs from three-dimensional wind and mass fields instead of using standard 850–200-hPa DLMs. The latter do not account for the variable vertical extension of individual storms and the flow governing their motion and may produce systematic position errors in barotropic models, as for example, in the 1996 cases Gustav, Josephine, and Marco. To examine these systematic biases, WBAR is subjected currently to tests with storm-dependent DLMs on the basis of three-dimensional Navy Operational Global Analysis and Prediction System input. The tests are carried out using a large number of tropical cyclone cases in all Northern Hemisphere ocean basins. Preliminary results corroborate the performance of WBAR during the 1996 Atlantic hurricane season and will be discussed in a subsequent paper. 2) Furthermore, the present track prediction system does not use all available datasets at a given base date/time. The inclusion of rawinsonde data, satellite cloud track winds, or special aircraft observations may have a positive impact on the performance of WBAR. 3) Finally, a further improvement might result from the execution of ensemble forecasts, for which barotropic models are particularly most suitable as a consequence of their computational efficiency. As discussed in section 3c, the performance of WBAR is sensitive to changes in the procedure to remove the contributions of azimuthal wavenumber one from the residual radial and tangential wind fields. Future tests will show whether statistical ensembles based on such model-inherent sensitivities can be used to further improve the present model performance.

Finally, a remark on some computational aspects of

[6] Computed using the best-track datasets described in section 2.

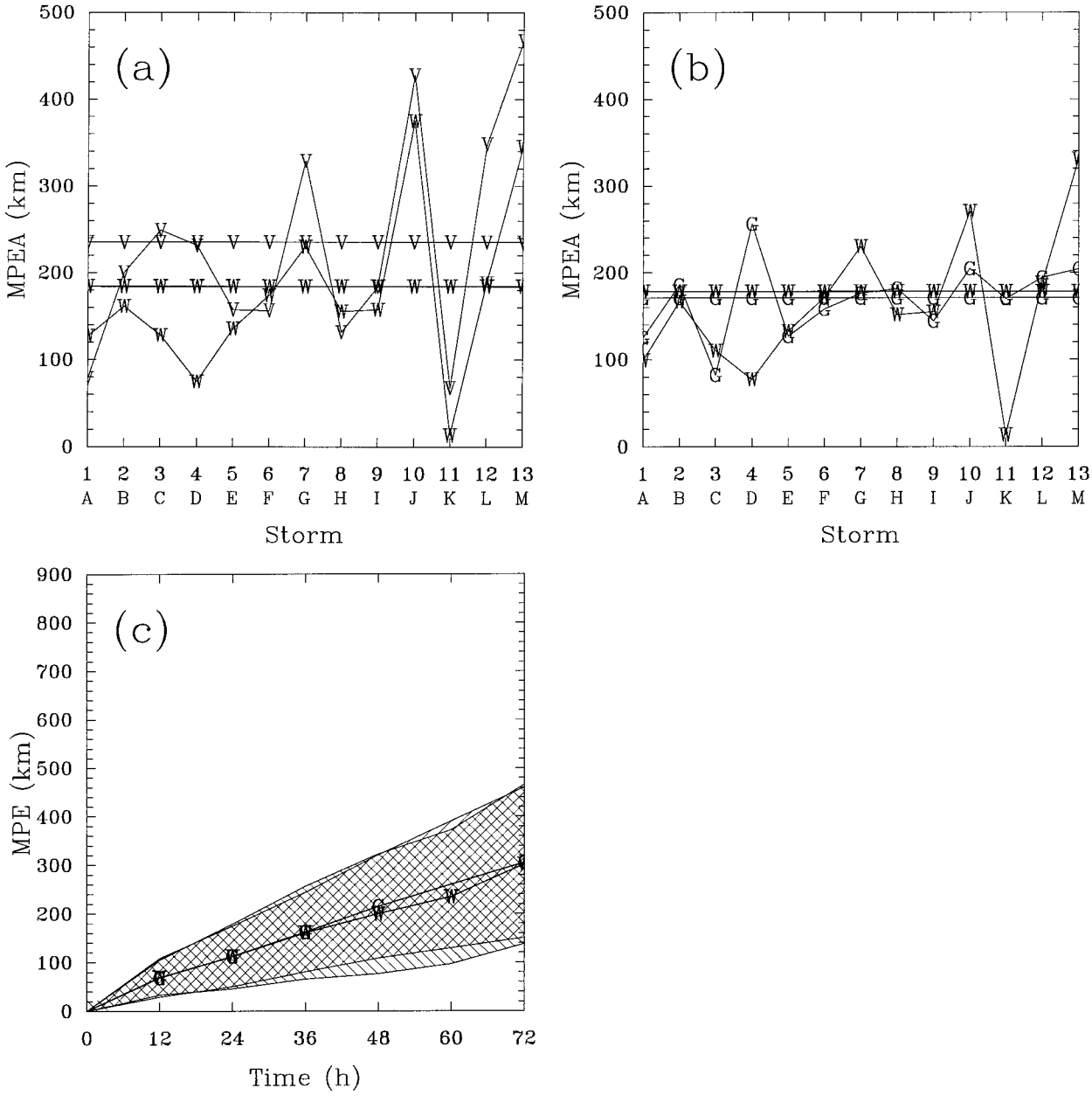

FIG. 9. Storm-by-storm MPEA in km vs all storms occurring in 1996 (e.g., the letter A below the abscissa represents Arthur etc.): comparison of WBAR (W) with (a) VICBAR (V) and (b) the GFDL model (G). The horizontal lines represent the MPEA of all storms in 1996. The number of cases used for the computation of the MPEAs corresponds with the number *N* given in the Tables 5b and 5c at 12-h prediction time. (c) As in Fig. 3c but without Dolly, Gustav, Josephine, and Marco.

WBAR: the present version is coded in standard FORTRAN 77 and was tested on a 1997 DEC Alpha Workstation (433 MHz, 196-MB RAM). In single-user mode, the real time required for one complete prediction cycle of WBAR on this machine, including postanalyses of the NCEP global model analyses and forecasts and a 72-h track prediction, is less than 5 min. The dependence of WBAR on temporal boundary conditions (cf. sections 2 and 4) such as those provided by the NCEP global model does not limit the portability of the new model: in order to adapt WBAR to a new data environment, only the necessary routines for reading the global input fields have to be replaced.

Acknowledgments. I wish to thank Dr. Sim Aberson for kindly providing the NCEP deep layer mean datasets, the TC advisories, and the track datasets of the operational prediction models used in this study. I also would like to sincerely thank Drs. Morris A. Bender, J. Dominique Möller, Lloyd J. Shapiro, Roger K. Smith,

and the second anonymous reviewer for their invaluable comments and suggestions. Last but not least, I am grateful for the financial support of the Office of Naval Research through Grant N00014-95-1-0394.

APPENDIX

Definitions of Statistical Quantities

The mean position error (MPE) at $t = t_0 + 12$, $t_0 + 24$, $t_0 + 36$, $t_0 + 48$, $t_0 + 60$, $t_0 + 72$ h is defined as

$$\mathrm{MPE}(t) = \frac{1}{N}\sum_{n=1}^{N} |\mathbf{x}_{pn}(t) - \mathbf{x}_{on}(t)|, \qquad \text{(A.1)}$$

where N denotes the number of available track predictions, $\mathbf{x}_{pn}(t) = (\lambda_{pn}, \varphi_{pn})$ the nth predicted position, and $\mathbf{x}_{on}(t) = (\lambda_{on}, \varphi_{on})$ the corresponding best-track position at time t. The position errors (PEs), $|\mathbf{x}_{pn}(t) - \mathbf{x}_{on}(t)|$, are computed using spherical geometry.

The mean position error of all prediction times (MPEA) is defined as

$$\mathrm{MPEA} = \frac{1}{6N}\sum_{i=1}^{6}\sum_{n=1}^{N} |\mathbf{x}_{pn}(t_i) - \mathbf{x}_{on}(t_i)|, \qquad \text{(A.2)}$$

where N denotes the number of available track predictions, t_i the ith prediction time (one of $t_0 + 12$, $t_0 + 24$, $t_0 + 36$, $t_0 + 48$, $t_0 + 60$, $t_0 + 72$ h), $\mathbf{x}_{pn}(t_i) = [\lambda_{pn}(t_i), \varphi_{pn}(t_i)]$ the nth predicted position at t_i, and $\mathbf{x}_{on}(t_i) = [\lambda_{on}(t_i), \varphi_{on}(t_i)]$ the corresponding observed position at time t_i. If less than six track preditions are available, the maximum summation index in Eq. (A.2) is reduced accordingly.

At a given prediction time, the mean skill S of a model A (index A) in comparison with a model B (index B) is defined as

$$S = \frac{100(\mathrm{MPE}_A - \mathrm{MPE}_B)}{\max(\mathrm{MPE}_A, \mathrm{MPE}_B)} \qquad \text{(A.3)}$$

in percent. A negative value of S (negative mean relative position error) represents positive skill of model A relative to model B. In this case, the absolute MPE of model A is less than that of model B. Equation (A.3) can be evaluated also using the PE at any given base date/time instead of the MPE.

At any given base date/time, the mean skill of all prediction times SA of model A (index A) relative to model B (index B) is defined as

$$SA = \sum_{i=1}^{6} \frac{100(\mathrm{PE}_A^i - \mathrm{PE}_B^i)}{\max(\mathrm{PE}_A^i, \mathrm{PE}_B^i)}, \qquad \text{(A.4)}$$

where PE^i represents the position error at time $t_i \in \{t_0 + 12, t_0 + 24, t_0 + 36, t_0 + 48, t_0 + 60, t_0 + 72$ h$\}$. As before, negative values of SA represent positive skill of model A relative to model B. In the case of less than six available track predictions, the maximum summation index in Eq. (A.4) is reduced.

REFERENCES

Aberson, S. D., and M. DeMaria, 1994: Verification of a nested barotropic hurricane track forecast model (VICBAR). *Mon. Wea. Rev.*, **122,** 2804–2815.

Bach, H., 1969: On the downhill method. *Commun. Assoc. Comp. Mach.*, **12,** 675–687.

Barnes, S. L., 1964: A technique for maximizing details in numerical weather map analysis. *J. Appl. Meteor.*, **3,** 396–409.

Bender, M. A., R. J. Ross, R. E. Tuleya, and Y. Kurihara, 1993: Improvements in tropical cyclone track and intensity forecasts using the GFDL initialization scheme. *Mon. Wea. Rev.*, **121,** 2046–2061.

Chan, J. C. L., and R. T. Williams, 1987: Analytical and numerical studies of the beta-effect in tropical cyclone motion. Part I: Zero mean flow. *J. Atmos. Sci.*, **44,** 1257–1265.

Davidson, N. E., and K. Puri, 1992: Tropical prediction using dynamical nudging, satellite-defined convective heat sources and a cyclone bogus. *Mon. Wea. Rev.*, **120,** 2501–2522.

——, and H. C. Weber, 2000: The BMRC high-resolution tropical cyclone prediction system: TC-LAPS. *Mon. Wea. Rev.*, **128,** 1245–1265.

——, J. Wadsley, K. Puri, K. Kurihara, and M. Ueno, 1993: Implementation of the JMA typhoon bogus in the BMRC tropical prediction system. *J. Meteor. Soc. Japan,* **71,** 437–467.

DeMaria, M., 1985: Tropical cyclone motion in a nondivergent barotropic model. *Mon. Wea. Rev.*, **113,** 1199–1210.

——, 1987: Tropical cyclone track prediction with a barotropic spectral model. *Mon. Wea. Rev.*, **115,** 2346–2357.

——, S. D. Aberson, K. V. Ooyama, and S. J. Lord, 1992: A nested spectral model for hurricane track forecasting. *Mon. Wea. Rev.*, **120,** 1628–1643.

Durran, D. R., 1991: The third-order Adams–Bashforth method: An attractive alternative to leapfrog time differencing. *Mon. Wea. Rev.*, **119,** 702–720.

Fiorino, M. J., and R. L. Elsberry, 1989: Some aspects of vortex structure related to tropical cyclone motion. *J. Atmos. Sci.*, **46,** 975–990.

Goldenberg, S. B., S. D. Aberson, and R. E. Kohler, 1985: Incorporation of Omega Dropwindsonde data into SANBAR: An operational barotropic hurricane-track forecast model. Preprints, *16th Conf. on Hurricanes and Tropical Meteorology,* Houston, TX, Amer. Meteor. Soc., 44–45.

——, ——, and ——, 1987: An updated, fine-grid version of the operational barotropic hurricane-track prediction model. Preprints, *17th Conf. on Hurricanes and Tropical Meteorology,* Miami, FL, Amer. Meteor. Soc., 86–89.

Grell, G. A., J. Dudhia, and D. R. Stauffer, 1994: A description of the fifth-generation Penn State/NCAR Mesoscale Model (MM5). NCAR Tech. Note NCAR/TN-398+STR, 138 pp.

Heming, J. T., and A. M. Radford, 1998: The performance of the United Kingdom Meteorological Office global model in predicting the tracks of Atlantic tropical cyclones in 1995. *Mon. Wea. Rev.*, **126,** 1323–1331.

Holland, G. J., 1983: Tropical cyclone motion: Environmental interaction plus a beta effect. *J. Atmos. Sci.*, **40,** 328–342.

Hope, J. R., and C. J. Neumann, 1970: An operational technique for relating the movement of existing tropical cyclones to past tracks. *Mon. Wea. Rev.*, **98,** 925–933.

Horsfall, F., M. DeMaria, and J. M. Gross, 1997: Optimal use of large-scale boundary and initial fields for limited-area hurricane forecast models. Preprints, *22d Conf. on Hurricanes and Tropical Meteorology,* Fort Collins, CO, Amer. Meteor. Soc., 571–572.

Kurihara, Y., M. A. Bender, and R. J. Ross, 1993: An initialization scheme for hurricane models by vortex specification. *Mon. Wea. Rev.*, **121,** 2030–2045.

——, ——, R. E. Tuleya, and R. J. Ross, 1995: Improvements in the GFDL hurricane prediction system. *Mon. Wea. Rev.*, **123,** 2791–2801.

——, R. E. Tuleya, and M. A. Bender, 1998: The GFDL hurricane prediction system and its performance in the 1995 hurricane season. *Mon. Wea. Rev.*, **126,** 1306–1322.

Lewis, J. M., C. M. Hayden, C. S. Velden, T. R. Stewart, R. J. Lord, S. B. Goldenberg, and S. D. Aberson, 1985: The use of VAS winds and temperatures as input to barotropic hurricane track forecasting. Preprints, *16th Conf. on Hurricanes and Tropical Meteorology*, Houston, TX, Amer. Meteor. Soc., 40–41.

Neumann, C. J., 1972: An alternate to the HURRAN tropical cyclone forecast system. NOAA Tech. Memo. NWS SR-62, 22 pp.

——, M. B. Lawrence, and E. L. Caso, 1977: Monte Carlo significance testing as applied to statistical tropical cyclone prediction models. *J. Appl. Meteor.*, **16,** 1165–1174.

Pasch, R. J., and L. A. Avila, 1999: Atlantic hurricane season of 1996. *Mon. Wea. Rev.*, **127,** 581–610.

Press, W. H., B. P. Flannery, S. A. Teukolsky, and W. T. Vetterling, 1986: *Numerical Recipes.* 1st ed. Cambridge University Press, 818 pp.

Ross, R. J., and Y. Kurihara, 1992: A simplified scheme to simulate asymmetries due to the beta effect in barotropic vortices. *J. Atmos. Sci.*, **49,** 1620–1628.

Sanders, F., and R. W. Burpee, 1968: Experiments in barotropic hurricane track forecasting. *J. Appl. Meteor.*, **7,** 313–323.

——, C. Pike, and J. P. Gaertner, 1975: A barotropic model for operational prediction of tracks of tropical storms. *J. Appl. Meteor.*, **14,** 265–280.

——, A. L. Adams, N. J. B. Gordon, and W. D. Jensen, 1980: Further development of a barotropic operational model for predicting paths of tropical storms. *Mon. Wea. Rev.*, **108,** 642–654.

Shapiro, R., 1970: Smoothing, filtering and boundary effects. *Rev. Geophys. Space Phys.*, **8,** 359–387.

Smith, R. K., 1991: An analytic theory of tropical-cyclone motion in a barotropic shear flow. *Quart. J. Roy. Meteor. Soc.*, **117,** 685–714.

——, and W. Ulrich, 1990: An analytical theory of tropical cyclone motion using a barotropic model. *J. Atmos. Sci.*, **47,** 1973–1986.

——, and H. C. Weber, 1993: An extended analytic theory of tropical-cyclone motion in a barotropic shear flow. *Quart. J. Roy. Meteor. Soc.*, **119,** 1149–1166.

Späth, H., 1990: *Eindimensionale Spline-Interpolationsalgorithmen.* Oldenbourg-Verlag, 391 pp.

——, 1991: *Zweidimensionale Spline-Interpolationsalgorithmen.* Oldenbourg-Verlag, 293 pp.

Surgi, N., H.-L. Pan, and S. J. Lord, 1998: Improvement of the NCEP global model over the Tropics: An evaluation of model performance during the 1995 hurricane season. *Mon. Wea. Rev.*, **126,** 1287–1305.

Swarztrauber, P., and R. Sweet, 1975: Efficient FORTRAN subprograms for the solution of elliptic partial differential equations. NCAR Tech. Note NCAR-TN/IA-109, 139 pp.

Ueno, M., 1989: Operational bogussing and prediction of typhoon in JMA. JMA/NPD Tech. Rep. 28, Japan Meteorological Agency/ Numerical Prediction Division, 49 pp.

Weber, H. C., and R. K. Smith, 1993: The stability of barotropic vortices: Implications for tropical cyclone motion. *Geophys. Astrophys. Fluid Dyn.*, **70,** 1–30.

——, and ——, 1995: Data sparsity and the tropical-cyclone analysis and prediction problem: Some simulation experiments with a barotropic numerical model. *Quart. J. Roy. Meteor. Soc.*, **121,** 631–654.